Annals of Materials Science & Engineering

Open Access

Austin Publishing Group

Review Article

A Review on the use of Graphene as a Protective Coating against Corrosion

Jianchen Hu[1]†, Yanfeng Ji[1]†, Yuanyuan Shi[1], Fei Hui[1], Huiling Duan[2] and Mario Lanza[1]*

[1]Institute of Functional Nano & Soft Materials, Soochow University, China

[2]Department of Mechanics and Engineering Science, Peking University, China

†These authors contributed equally to this work

***Corresponding author:** Mario Lanza, Institute of Functional Nano & Soft Materials, Soochow University, China

Received: September 18, 2014; **Accepted:** October 26, 2014; **Published:** November 01, 2014

Abstract

Graphene was synthesized for the first time one decade ago and, during this time, the structure and properties of graphene have been well defined by many scientists. In parallel, some new graphene-based devices appeared, such as graphene field effect transistors, supercapacitors and micro electromechanical systems. Now is the moment to start exporting all these prototypes from the laboratory to the industry to move forward the technology. Such task will suppose a huge effort and will be accompanied by the necessary reliability tests to assess the lifetime of the new products, which will unavoidably generate important delays. On the other hand, among all applications of graphene, one may see the light faster than the others due to its simplicity: the use of graphene as protective coating. It has been demonstrated that the ultra-dense network of carbon atoms that form graphene is totally impermeable to protect a material from corrosion, and at the same time it is so thin that keeps unaltered the chemical properties of the protected material. In this review, we analyze the anti-corrosion properties of graphene and debate about its viability in near-future applications.

Keywords: Graphene; Local oxidation; Corrosion resistance; Stability; Ageing mechanisms

Introduction

Before its appearance, there was a debate on the possibility of graphene viability, and a consensus existed on that crystalline two dimensional (2D) materials would rapidly decompose under room temperature depending on their intrinsic thermodynamic instability [1-3]. In 1966, a theory was proposed by Mermin and Wagner describing the destructive impact of wavelength variation to the long-term orderly 2D crystalline materials [4]. Therefore, graphene was just proposed as an established ideal theoretical model for studying carbonaceous materials and did not receive its deserved attention. In this context, the experimental synthesis of graphene in 2004 [5] was a huge surprise to the world.

Ideal graphene can be considered as a single-atom-thick sheet made of carbon atoms arranged in a hexagonal honeycomb lattice, in which each carbon atom is a sp^2-hybridized point and denotes an electron from *p* orbital forming a π-bonding [6-9]. This unique structure endows graphene an extraordinary combination of mechanical [10,11], physical [12,13], electronic [14,15], chemical [6], and optical [16] properties, and even other more exotic properties such as wetting transparency [17] have been also reported. The strong physico-mechanical performance comes from the high stability of the covalent bonds between the carbon atoms [6], while its superior electronic properties are related to the cloud of free carriers available on its surface [9]. At the same time, graphene is the thinnest material possible and, therefore, almost completely transparent [16].

Due to its incomparable high electron mobility, graphene has raised most interest in the field of microelectronics. The earliest synthesis of monolayer graphene in 2004 had showed an electrical conductivity of 1×10^4 $cm^2/V\bullet s$, which was much higher than that of the contemporary transistors (~1400 $cm^2/V\bullet s$) [5]. Mayorov and co-workers [15], improved the conductivity to 2.5×10^5 $cm^2/V\bullet s$ using encapsulated graphene. Another advantage of graphene is that its electrical conductivity is not influenced by the temperature variation [18,19]. Normally, increased temperature causes crystal lattice vibration and electrons are scattered, leading to a decrease of conductivity. But this does not occur to graphene because fewer electrons are scattered and temperature does not impact on this result. It was proved that the conductivity of graphene can be kept as 1.5×10^5 $cm^2/V\bullet s$ in temperatures ranging from 50 K to 500 K [18].

Apart from its electronic magnificence, other physical properties of graphene are also very attractive. Graphene has a high mechanical strength of 1100 GPa (Young modulus) and breaking strength of 125 GPa which is close to that of carbon nanotube, 100 times larger than a sheet of steal with similar thickness [20]. In other words, graphene is the material with the highest strength on earth; and at the same time, it is flexible. Tensile stresses have reported that graphene can be elongated 23% without inducing cracks or fracture [21]. Graphene thermal conductivity up to 5000 $W/(m\bullet k)$ has been reported [12,13], which is 5 times higher than that of diamond, the material that showed previous best performance. Furthermore, graphene can be used as blocking barrier, since no material can penetrate its dense lattice structure, including the smallest atoms of Helium [24]. Moreover, graphene is transparent; the optical absorption of a single graphene layer is shown to be ~2.3% over the visible spectrum [16], which combined with its high electrical conductivity, could lead to transparent conductive electrodes [25-27]. But as the most basic physical property, the melting point of graphene has never been experimentally demonstrated.

The attractive performance of graphene in the field of chemistry relies on its large surface area. Values of surface areas of 2630 m^2/g

Citation: Hu J, Ji Y, Shi Y, Hui F, Duan H and Lanza M. A Review on the use of Graphene as a Protective Coating against Corrosion. Ann J Materials Sci Eng. 2014;1(3): 16.

have been systematically reported [28-30]. Since chemical reactions are promoted by the atoms at the surface of a material, graphene is very suitable for exhaustive promotion of chemical reactions. At present, it is known that the surface of graphene is similar to that of graphite, which has abilities of absorption and desorption to some atoms and molecules, like NO_2, NH_3 and K [31-36]. The absorbates normally play the role of an electron acceptor, causing a decrease of graphene's conductivity. Graphane was the first functionalized graphene derivative, in which each carbon atom was bonded with a hydrogen atom [37]. Other functional groups are also candidates for functionalizing graphene to explore new applications. As a comparable example, the graphite sheets formed by un-functionalized graphene are porous and fragile, but the counterparts made of compactly oxidized graphene are truly hard and coriaceous [38,39]. The chemical treated graphene has many potential applications, but the lack of production for traditional treatments is a bottleneck.

Apart from the intrinsic properties of graphene, other capabilities may be engineered by intentionally altering its structure. For example, graphene is not a piezoelectric material but atomistic calculations predicted that covering graphene surface with specific elements may lead piezoelectric coefficients to reach a nontrivial maximum, which can be attributed to abrupt charge transfer from graphene to the dopants [40]. Li et al. [41] functionalized graphene by modification of graphene with potassium (K) using a room-temperature chemical method and made K-modified graphene act as an electron transfer medium, promoting charge transfer more efficiently than unmodified graphene.

By looking at the properties of graphene one could think that a very complicated process may be necessary to fabricate it, but in fact graphene was synthesized for the first time by utilizing a very simple method. Novoselov et al. [5] stick a flake of graphite to tape and then exfoliated it to separate the graphite layers, and repeated this process for many times to reduce the thickness of the remaining graphite on the tape, until a few layers graphene sheet was successfully isolated. But the shortage for this technique is the difficulty to obtain large-area sheets with controllable thicknesses, which is a mandatory requirement for mass production. The unprecedented interest raised by graphene led to the rapid development of new fabrication methods, such as ultrahigh vacuum (UHV) annealing of single crystal SiC [42,43], chemical vapor deposition (CVD) [44-50], liquid-phase exfoliation of graphite [51], unzipping of single-wall carbon nanotubes [52] and molecular assembly [53]. Among them, CVD graphene has showed the best quality-price ratio and, therefore, is one of the most promising for new graphene devices fabrication. Many carbon-source gases can be employed to prepare graphene in CVD system, such as methane (CH_4) [54], acetylene (C_2H_2) [55], ethanol (CH_3CH_2OH) [56], benzene (C_6H_6) [57] and cyclohexane (C_6H_{12}) [58], among others. The injected carbon source gas or gases can be reduced by H_2 or decomposed under high temperature (~1000^{O}C) in the oxygen-free CVD system, and graphene sheets with controllable thicknesses can be deposited on many substrates, like Cu [50,59], Ir [60], Ru [46], Ni [49,61], Pt [62]. Besides, the size of graphene fabricated in CVD can be reached to several centimeters [63], and for some kinds of substrates it is easy to transfer to arbitrary samples [64]. Recently Wang et al. [65] demonstrated large-scale and uniform deposition of high-quality graphene directly on a wafer-scale Ge substrate and has been considered to replace conventional Si for the next generation of high-performance metal-oxide-semiconductor field-effect transistors (MOSFETs).

An alternative way to produce graphene is starting from graphene oxide (GO). Dikin et al. [66] firstly reported a reduction process to fabricate graphene by reducing GO with injected hydrazine. The highly ordered structure of graphene was recovered by this process, and the yield was comparable to that produced by physical techniques. However, it is difficult to reduce the original graphene oxide fully, leading to a residual dispersed in the formed graphene that impoverishes its properties, eg. conductivity. Various previous attempts give guidance to improve this redox process; the most notable were reported by Standenmaier [67], Brodie [68] and Hummers [69]. The common principle of these improved redox methods is that, since the stacking space (0.7~1.2 nm) of GO is larger than that of graphene (~0.34 nm), it is easy for other molecules to insert in. Thus, strong protonic acid can be introduced to treat GO, forming composite between the GO layers and then be oxidized [70]. After a reduction process, high quality graphene can be produced.

The combination of all these properties and fabrication methods may lead to a new generation of devices [71], from flexible and transparent electronic devices, to high-performance batteries and chemical filters, and after a decade analyzing its properties, now is the moment of bringing this exciting material to the industry. To date, the only companies making real profit with graphene are those who commercialize the raw material. One of the easiest and most immediate applications for graphene is as protective coating against corrosion. In such case, graphene doesn't need to be patterned by lithography, and just needs to be transferred on the material to be protected. In this work, we review the progress on graphene as protective coating against corrosion, and a deep discussion about oxidation resistance of graphene will be presented. After the introduction, in section 2 we summarize the most promising applications of graphene as protective coating, and we describe the role that the graphene sheets play in each case. In section 3, the physics and chemistry behind the protective effect are discussed, mainly focusing on three properties: impermeability, anti-oxidation barrier and water transparency. Furthermore, the use of graphene as anti-oxidation coating and the ageing of graphene coated materials under oxidative environments are presented, in sections 4 and 5 respectively. Finally, section 6 provides a prospect section where we debate the future use of graphene as protective coating.

Applications

The applications of graphene range from electronics to nanomedicine, including micro electromechanical systems, information storage, optoelectronics, plasmonics, batteries, clean energy harvesting, solar cells, chemistry, industrial protective coatings, filters, sensors, actuators and biotechnology. In the next sections we highlight outstanding examples with immediate applications in the industry.

High frequency transistors

Graphene high carrier mobility has been used in radio-frequency (RF) electronics [72-77]. Han et al. [78] created an amplifier with low output conductance of 0.1 mS/μm showing evidences of realistic

potential for graphene field effect transistor (GFET) and advanced RF circuitry. GFETs' working principle is different to conventional semiconductor FETs: graphene is gapless so that it is hard to saturate by conventional means, in which drain current saturation relies on energy band gap. Although it brings up an excellent performance in conductance and migration rate, it can also introduce severe defects that weaken the device performance. Liao et al. came into an approach of high-speed graphene transistor with a self-aligned nanowire gate [79], which could prevent the defects of monolayer carbon lattices in the conventional device fabrication. The transistor showed high scaled on-current of 3.32 mA/μm and transconductance of 1.27 mS/μm with an ultrahigh intrinsic cut-off frequency of 100-300 GHz.

Capacitors and energy storage

The social development and ecological concern have accentuated the need of environmental friendly energy storage systems [80]. However, conventional batteries and fuel cells have deficiencies like low energy densities [81], short cycle life, slow charging and discharging at high densities, some of which could be satisfied with carbon-based devices. Although carbon nanotubes (CNTs) show excellent conductivity and high surface areas, they may contain defects between electrode and current collector [82,83]. In this direction, graphene emerged as promising electrode for charge storage due to its high surface area, which depends on the graphene layers rather than the distribution of porous in carbon nanotube. Wang et al. [84] obtained a maximum specific capacitance of 205 F/g at 1.0 V in aqueous electrolyte with energy density of 28.5 Wh/kg, which is significantly higher than those of CNT-based supercapacitors [30,85]. Such supercapacitors represent a realistic solution for energy storage.

Moreover, graphene is useful for hydrogen storage. Hydrogen is one of the cleanest energy sources, but a reliable hydrogen-based technology requires solving the issue of storage and transportation. The conventional method of storing containers is a bottleneck to the advancement of hydrogen technologies [40,86-93]. Nanocomposite alloys have shown the capacity of storing hydrogen, and $LaNi_5$, TiFe and MgNi (among others) have showed decent performance. In such materials, La and Ti alloys are low temperature hydrogen storage materials with low capacity, while Mg alloys are high temperature hydrogen storage materials. Although the theoretical capacities are high, the dynamics of adsorption and desorption is unstable. Moreover, alloys are expensive and have a high density, which limits their application. Ghosh et al. [94] found that three-four layers of graphene have a higher performance to adsorb H_2 and CO_2. The uptake of H_2 is up to 1.7 wt% at a pressure of 1 atm and a temperature of 77 K. It should be possible to increase it by reducing the average number of graphene layers. It has been suggested that the single-layer graphene would show as high as 7.7 wt% of uptake [94]. Such experiments support the theory that graphene is an excellent material for hydrogen storage.

Biology

Graphene biologic sensors are necessary because they may provide enhanced capabilities. For example, graphene may allow fabricating biologic sensors and actuators, and its ultra-high conductivity may result in an extraordinary accuracy. The most studied sensors are those that monitor pH values. The work of Ang et al. [95] showed that few layer graphene can be used as pH sensors with ultrafast performance and ultralow noise. The oxygen-containing groups on the surface of graphene can form hydrogen bond with hydroxyl (OH^-) and hydroxonium ions (H_3O^+). One or two layers of epitaxial graphene can effectively sense the density of ions from the interface. They have been successfully observed in the solution-gating of epitaxial graphene, where ambipolar characteristics with a narrow *p-n* plateau region (~ 0.2 eV) near the Dirac point have been measured. Both *n* and *p* carriers can be induced from graphene/electrolyte interface, with the negative gated potential region exhibiting supra-Nernstian response to pH.

Graphene-based gas molecule sensors are also interesting due to their excellent sensitivity, which is possibly thanks to graphene exceptional low-noise [96]. For traditional materials, increase of temperature results on a conductivity decrease, leading to intrinsic noise and limiting resolution of common sensors [97]. But this does not apply to graphene. Furthermore, graphene can absorb gas molecules that can act as electron donors or acceptors, resulting in variation of conductance. Its effect is surprising even to solid-state gas sensors: Schedin et al. [96] showed micrometer-size sensors made from graphene and reported adsorption of NO_2, NH_3, H_2, CO. They obtained the lower detection to 1 ppm (parts per million) and an apparent variation of conductance in 1 min. Sundaram et al. [98] investigated the effect of nanoparticles on graphene. The electrochemical modification of a controllable density of Pd particles on graphene monolayers can effectively enhance the hydrogen sensitivity. Liu et al. [99] discovered a unique ability of graphene in attachment and delivery of aromatic, water insoluble drugs.

Chemical filters

According to molecular dynamics, carbon nanotubes could transfer gas and liquid. Hydrated ions could also go through carbon nanotubes with bigger radius. Sint and co-workers [100] designed functionalized nanopores in graphene monolayers and found that they can be a passage for hydrated ions. For example, fluorine–nitrogen terminated pores selectively let Li^+, Na^+, K^+ go through, but not anions, with rates around 9:14:33. Molecular dynamic simulations show that the Hydrogen-pores can only be passed by irons of Cl^- and Br^- with ratios of 17:33. That means the nanopores are selective to iron polarity. Simultaneously, they found that the pores work on different size of ions, which can be deduced from the lowest rates of Li^+ and F^-. Therefore, these nanopores could be useful in molecular separation and desalination. Despite the use of graphene in this field is still in its embryonic stage, it is worth to be highlighted due to the tremendous impact it would have in hot fields like water purification.

Micro and nano electromechanical systems

The application of graphene in the field of micro and nano electromechanical systems (MEMS and NEMS) has attracted considerable attention due to the additional capabilities and performance graphene may provide. One of the novel graphene-based MEMS that attracted most interest in the last years is graphene-coated tips for electrical modes of atomic force microscope (AFM) [101]. Traditionally, metallic varnishes were used to provide the conductivity capability to the bulk silicon AFM tips [102]. Despite the considerable performance increase provided by such varnishes, the tips can still wear out quickly when measuring high currents due to thermal heat. Violent tip-sample friction during scans in contact

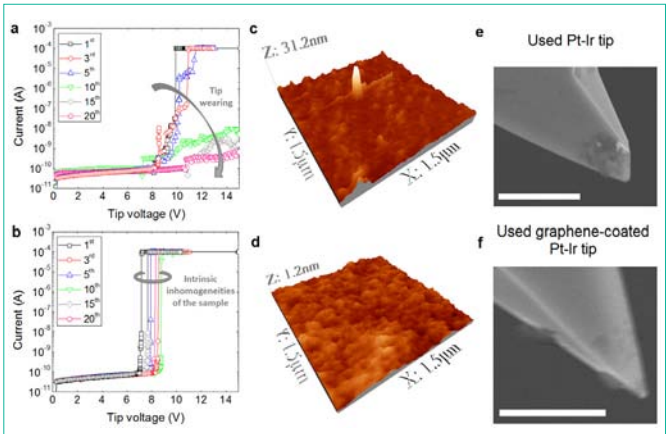

Figure 1: I-V curves collected from the bare surface of HfO_2/SiO_2 stack using (a) a pristine tip, (b) a graphene-coated tip. Each image contains the 1st, 3rd, 5th, 10th, 15th, and 20th measurements. (c) and (d) show the topographic maps after reaching the dielectric breakdown (DB) with a non-coated tip and a graphene-coated tip, respectively. (e) and (f) are SEM images of Pt-Ir tip and graphene-coated Pt-Ir tip after the 20 I-V curves and one topographic scanning, respectively. The scale bars in (e) and (f) are 5 μm and 3 μm, respectively. Reproduced with permission from Ref [101]. Copyright 2013 WILEY-VCH Verlag GmbH & Co. KGaA, Weinheim.

mode can also lead to premature tip damage, which will result in false imaging due to sample contamination. Moreover, premature tip wearing tremendously increases the cost of research. Even if doped-diamond coated tips apparently showed better performance, they can reduce the lateral resolution as well as increase the price of the tips. Therefore, finding an excellent method to enlarge the lifetime of the tips is necessary. And in this field, graphene may play a strategic role due to its excellent properties and stability [103].

The first graphene-coated AFM tip was reported in 2012 by Wen et al. [104], who used it as electrode in molecular junctions. In that work, multilayer graphene sheets were directly grown on Au-varnished CAFM tips by following the CVD process (i.e. the metal-varnished tip was introduced in the CVD furnace). Wen's prototypes got a high yield with a relative simple process, indicating that the mass production of graphene tips for AFM-based applications could be feasible. Despite the good performance reported by the authors, the quality of the graphene grown on the metallic varnish of the tip may not be as good as the one of the optimized GSL on Copper foils. Another approach is to grow a continuous layer of graphene in pre-patterned substrates. Martin-Olmos et al. [105] grew a layer of graphene in a copper mold and filled it with SU-8 resist. Using that method, the authors proved high yield and enhanced functionality of the tips, observing a larger conductivity and a higher lifetime. The main problem of this method is that, unlike Wen's prototype, it requires a completely new fabrication process (i.e. it doesn't starts from a terminated product), which drastically increased its cost. Shim et al. [106] used for the first time a multilayer graphene coating to fabricate multifunctional parallel probe arrays with high resistance to wear, sharpness and high electrical and thermal conductivities. Such prototype was successfully used in the field of scanning probe lithography techniques.

In our previous work [107], a sheet of GSL grown on Copper was transferred onto different Pt-Ir vanished CAFM tips, and the novel prototypes were used to characterize the electrical performance of both conductive substrates and thin insulators on Silicon. The coating process consisted of: i) fixing the tip on a piece of silicon wafer using a thin film of Poly-methyl methacrylate (PMMA) below and on it; ii) the integral PMMA/AFM-tip/PMMA/Silicon block was used as a solid substrate on which the graphene sheet was transferred; and iii) removing each PMMA layer using acetone (which took 30 min, while a normal one needs only 5min). When the PMMA is eliminated, GSL is completely attached to the tip by van-der-Waals forces.

As a standard sample in nanoelectronics [108-116], we used HfO_2 (3nm)/SiO_2 (1nm)/Si (n-doped) stacks to analyze the performance of graphene coated tips. Figure 1 shows the 1st, 3rd, 5th, 10th, 15th, and 20th I–V curves measured on the bare surface of HfO_2/SiO_2/Si stack at different random fresh positions of using a pristine Pt-Ir tip (Figure 1a) and a graphene-coated tip (Figure 1b). As it can be observed, the current decreases in figure 1a with the number of voltage ramps, indicating that the tip worn out at high current densities ($J \approx 10^8$ A/cm^2 when it reaches the current compliances (CC), that is 100μA through an area of 100 nm^2). On the contrary, the graphene-coated tip undertakes many measurements (Figure 1b), which entirely reached the CC level roughly at the same onset voltage without assessable wearing. The apparent differences in figure 1b are related to the intrinsic in homogeneities in the HfO_2 film, as observed in other thin oxides [108-116].

We scanned the surface of the sample before and after the dielectric breakdown (DB) to study the tip wearing effect. Figures 1c and 1d show the topographic CAFM images of samples scanned with as-received tip and graphene-coated tip after the DB event, which was induced previously by ramped voltage stresses. As the images show, at fresh areas (surrounding parts of the map) the topographies of both images are in the range of 2 nm [117], while the clear difference can be seen at the areas where DB was triggered (central area). The high hillock of 31.2 nm shows up using as-received tips (Figure 1c), a reported phenomenon known as dielectric breakdown induced epitaxy (DBIE) that is related to the violence of the uncontrolled DB [118]. Note that, these phenomena are especially harmful to the CAFM tips when inducing the DB due to the instability of the CAFM tip metallic varnish [119]. Platinum and Iridium atoms from the tip can break their bonds and penetrate in the insulating layer, which will not only destroys the tip, but also contaminates the samples, indeed providing untrue electrical and topographic data. On the contrary, when the DB is induced using graphene-coated tips no surface modification is observed. Graphene-coated tips successfully avoid the tip-sample interaction during the DB event, which would interest many researchers in the field of resistive switching. At the same time, SEM images also demonstrate the extremely low wearing of graphene-coated tips. Figures 1e and 1f show the SEM images of both Pt–Ir and graphene-coated Pt–Ir tips after 20 I-V curves and one topographic map. It is evident that the as-received tip can wear out easily due to the high currents, while the graphene-coated tip remains with the same shape (and high conductivity).

The capabilities of the tips fabricated by this method were further corroborated in our further report in Ref. [120]. In that work, an enhanced resolution of the tips is reported, this may be related to the presence of a nanogap between graphene and the tip apex. Such phenomenon may reduce the tip radius and tip-sample contact area.

Electrochemical cells

The ability of graphene to protect underlying materials has also been extended to other fields. As an example, GSL sheets have demonstrated corrosion resistance to electrochemical cells. Traditional electrochemical devices such as water splitting cells (among others) used metallic corrosion-resistant coatings. Chen et al. [121] reported Iridium corrosion-resistant nanocomposite for the oxidation of water. But the problem related to this work is the high cost of the Iridium. The breaking work of Kenney et al. [122] showed that deposition of a thin and inexpensive layer of nickel film on n-type silicon (n-Si) affords active and durable oxygen evolution reaction (OER).

Graphene has been shown to be a potential alternative, offering notable degrees of protection. Chen et al. [123] reported a combined reduced graphene oxide (rGO)/TiO_2 on top of Fluorine-doped Tin Oxide, which showed better performance than the same device without rGO, with a power conversion efficiency (PCE) from 5.8% to 8.13%. Furthermore, graphene is also a good photoanode, replacing semiconductor oxides. As shown by Anish et al. [124], the PCE can be improved from up to 12% by mixing TiO_2 with graphene derivative. In addition, graphene can be used in the counter electrode, which dictates the cathodic activity and alters the performance by regulating the restoration of redox couple. Lee et al. reported the performance of a graphene-based 3D nano-foam, which showed short-circuit current density of 12.1 mA/cm^2, and open circuit voltage of 0.7 V, respectively. Chen et al. [125] got an even higher efficiency with a similar system.

Furthermore, Dhiraj et al. [126] demonstrated that graphene could effectively protect underlying metals from corrosion in electrochemical assays. As an example, Figure 2(a) shows the cyclic voltammograms (CV) collected on Cu foils with and without graphene protection. The CV curves show four peaks compatible with these reactions. The cathodic current decreases when the potential is less negative, extending with an anodic peak at 150 mV (Potential vs. Ag/AgCl), which results from species formed on the bare surface of Cu. These adsorbed species can be subsequently dissolved by quartz crystal microbalance (QCM) and rotating ring-disk electrode (RRDE) experiments [127]. The three cathodic peaks at 0, 250, and 550 mV, which are related to electroreduction of copper ions, can also be observed. On the contrary, the Gr/Cu samples show no peaks in the CV process and exhibit extremely low current at positive potentials. It is convincing that GSL provides a valid barrier holding back the corrosion of the copper surface. In order to get more information about the nature corrosion, SEM images are obtained in Figure 2b, showing the Cu and Gr/Cu samples before and after CV scan. As it can be observed, the surface of bare Cu is entirely damaged after the CV process (200 mV from the open circuit potential, OCP), while in Gr/Cu samples most areas keep the original state, only some isolated areas degrades. That is, the corrosion occurred at the areas uncovered by graphene, which means single layer graphene can serve as corrosion-inhibiting coating to protect the underlying metal.

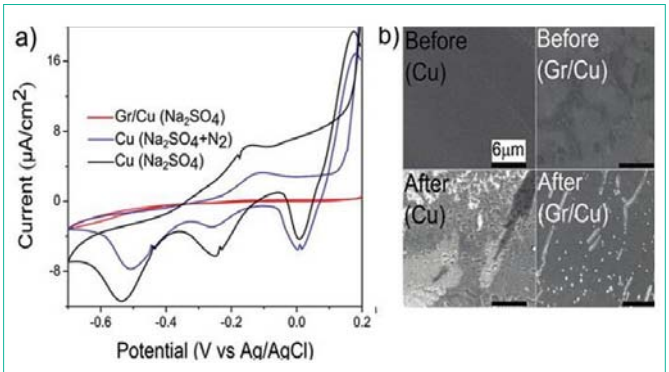

Figure 2: (a) Cyclic voltammetry curves of bare Cu and Gr/Cu samples in the electrolyte of 0.1 M Na_2SO_4. Blue line is measured with nitrogen bubbled in the solution. (b) SEM images of Cu and Gr/Cu samples before and after CV scan. Reprinted with permission from Ref. [126]. Copyright 2012 American Chemical Society.

Stability of Graphene

Among all the properties of graphene, the one that seems to have a more immediate application for the industry is its stability. More specifically, graphene has been shown to be a good anti-corrosion and anti-oxidation layer. The use of graphene in this field is one of the easiest possible, since it doesn't need any additional treatment, device pattern or lithography, and just the raw material should be grown on transferred on the one to protect. This industry-friendly application may be the motor field for the introduction of graphene in mass consumables. In this section we analyze the stability of graphene from three different points of views by highlighting notable reports related to graphene stability.

Impermeability

From the point of view of impermeability, graphene can be understood as a nanometric shield which can effectively withstand the wear produced by invasive agents from ambient. The hexagonal network of carbon atoms in graphene is so dense that no known material can penetrate it. Bunch and co-workers [24] described graphene as a membrane that could block transferring gas molecules. In their work, the graphene film could withstand a pressure difference larger than one atmosphere. Figure 3a schematically shows a graphene-sealed SiO_2 microchamber. Graphene thickness was altered from 1 to ~75 layers, which was proved by Raman spectra [128,129]. The graphene film was able to stick to the microchamber side walls by van der Waals force between graphene and SiO_2, forming a gas package with a size of ~μm^3. The inset in Figure 3a shows a 4.75 μm × 4.75 μm squared graphene sheet sealing the top face of the microchamber. The pressure difference Δp was defined as the difference value of the inside pressure (p_{int}) (atmospheric pressure, 101 kPa) and the external pressure (p_{ext}) of the microchamber is $\Delta p = p_{int} - p_{ext}$. If p_{ext} is changed, p_{int} would become to a balance state to p_{ext} because of relaxation effect, and the relaxation time could be varied from minutes to days depending on the gas species and the temperature.

For times shorter than the equilibration time, an apparent pressure difference Δp can exist across the membrane, causing it stretching like the surface of a balloon (Figure 3b). Situations for $\Delta p>0$ and $\Delta p<0$ are shown in Figure 3c and Figure 3d, respectively. The authors successfully created a positive pressure difference, $\Delta p>0$ and a lower pressure in the chamber ($\Delta p<0$), and observed the images of the membrane bulges upward and deflected downward by tapping mode atomic force microscope (AFM), respectively. Figure 3e shows results for different membranes of altered thicknesses and for different gases: air, argon and helium. Each gas showed no noticeable

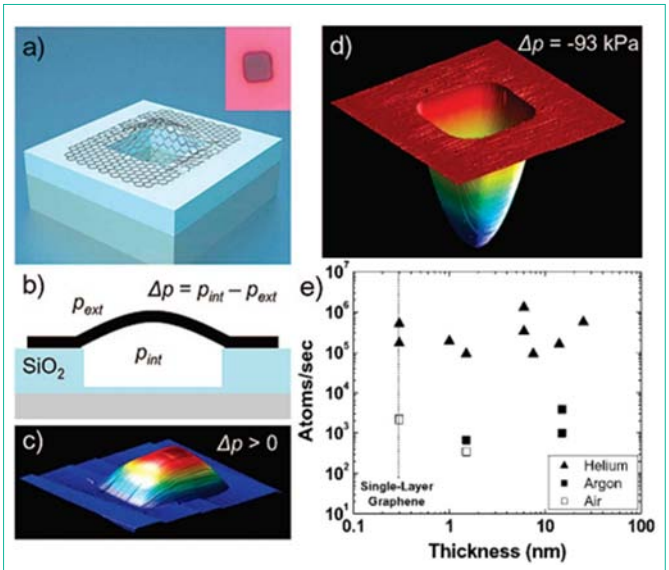

Figure 3: (a) Schematic of a graphene sealed microchamber. (Inset) optical image of a single atomic layer graphene drumhead on SiO_2. (b) Side view schematic of the graphene sealed microchamber. (c) AFM image of a ~ 9 nm thick many-layer graphene drumhead with Δp > 0. (d) AFM image of the graphene sealed microchamber of Figure 3a with Δp= -93 kPa across it. (e) Relationship of the gas leak rates *vs*. thickness: Helium (▲), argon (■) and air (□). Reprinted with permission from Ref. [24]. Copyright 2008 American Chemical Society.

dependence on thickness from 1 to 75 atomic layers under the situation of approximately same pressure difference applied across the membrane, indicating that the leak was neither through the graphene sheets nor though defects in these sheets. This suggests glass walls of the microchamber or the graphene-SiO_2 sealed interface should be responsible to the gas leak [130]. This offers the opportunity to probe the permeability of gases through atomic vacancies in single layers of atoms [131] and defects patterned in the graphene membrane, acting as selective barriers for ultrafiltration [132,133].

Anti-oxidation barrier

Graphene has also shown the ability of protecting some materials from oxidation. Chen et al. [134] used as-grown graphene in CVD system for the first time to protect Cu or Cu/Ni alloy surfaces from oxidation. The introduction of this protection layer led a passivation of the metal or metal alloy underneath. Our recent publication [107] proved that graphene transferred from original growth substrate to the target substrate also has passivation effect. The earlier discussed impermeability [24] is one of the aspects responsible to the passivation since the covering graphene offered an inserted block between the reactants and the protected metal or metal alloy. In other words, a solid film barrier was provided to separate the environment and the metal surfaces physically. On the other hand, the employed barrier layer should be chemically inert in the active oxidation environments [135]. Therefore, the stability of graphene in wild oxidation environments is another important consideration for its further applications. To investigate and verify graphene's chemical stability, graphene-covered Cu and Cu/Ni samples were exposed in accelerated oxidative environments, one of which was lengthy air anneals (200°C, 4 h) and the other one was hydrogen peroxide (H_2O_2, 30%, 2 min). Figure 4a schematically shows that the graphene film played the role of a molecular diffusion barrier, keeping the reactive agent away from the metal underneath. Interestingly, as a vivid example, comparison was carried out between two penny coins (95%Cu/5%Zn), one of which was coated by graphene monolayer and the other was naked. H_2O_2 treatment was introduced to these coated and uncoated coins. As shown in Figure 4b, the uncoated copper penny showed a color change caused by oxidation, whereas the graphene-coated coin kept the appearance like its original.

X-Ray Photoelectron Spectroscopy (XPS) analysis was able to monitor elemental variations before and after heating (200°C, 4 h) in both graphene-coated and uncoated Cu and Cu/Ni substrates. Before air annealing, original graphene-coated and uncoated Cu possessed same sharp peaks in their XPS spectra, at binding energies of 932.6 and 952.5 eV , which has been proved corresponding to $Cu2p_{3/2}$ and $Cu2p_{1/2}$ [136,137]. Importantly, after air annealing the graphene coated Cu foil maintained the same two sharp peaks, but the uncoated Cu received broader peaks combined with binding energies of different copper oxides, Cu_2O (932.5 and 952.3 eV), CuO (933.6 and 953.4 eV), and $Cu(OH)_2$ (934.7 and 954.5 eV) [130,131] (Figure 4c). As convincing evidence, a Raman spectrum was employed in order to confirm which new materials formed after treatment (Figure 4e). A small G/2D peak ratio (~0.5) of the coated Cu foil before treatment indicated the high quality single layer graphene [129]. On the contrary, after heat treatment multiple peaks between 214 and 800 cm^{-1} appeared to the uncoated Cu foil, supporting the existence of various copper oxides: Cu_2O (214, 644 cm^{-1}), CuO (299, 500 cm^{-1}), and $Cu(OH)_2$ (800 cm^{-1}) [138,139] (Figure 4e). Similarly, the same phenomena were observed on the graphene-coated and uncoated

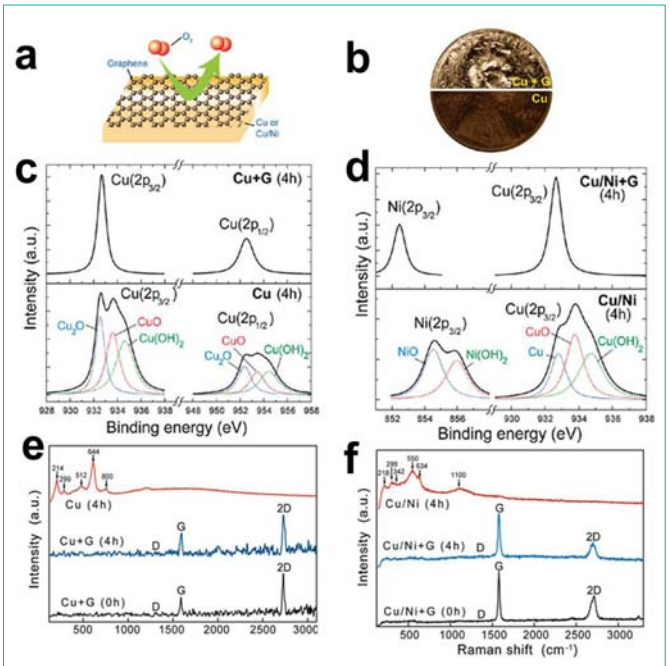

Figure 4: (a) Schematic of a graphene sheet as a chemically inert diffusion barrier. (b) Image of a penny coated (upper) and uncoated (lower) with graphene after treated in H_2O_2 for 2 min (30%). (c) XPS core-level Cu2p spectrum of coated (upper) and uncoated (lower) Cu foil after air anneal (200°C, 4 h). (d) XPS core-level $Ni2p_{3/2}$ and $Cu2p_{3/2}$ spectrum of coated (upper) and uncoated (lower) Cu/Ni foil after air anneal (200°C, 4 h). Raman spectrum of the (e) Cu and (f) Cu/Ni alloy foils with and without a graphene coating after air anneal (200°C, 0 and 4 h, respectively) Reprinted with permission from Ref. [134]. Copyright 2011 American Chemical Society.

Cu/Ni substrates. As shown in Figure 4d, two sharp XPS peaks corresponding to $Cu2p_{3/2}$ (932.6 eV) and $Ni2p_{3/2}$ (852.5 eV) [136] are present, demonstrating no elemental variation in the protected metal. As before, uncoated foil reveals two broader peaks, one of which is combined with two nickel oxide peaks, NiO (854.5 eV) and $Ni(OH)_2$ (856.0 eV), [136,140] and the other is composed of the peaks of metallic Cu (932.6 eV) and two copper oxide peaks, CuO (933.6 eV), and $Cu(OH)_2$ (934.7 eV). These XPS spectra indicate that the naked Cu/Ni foil was certainly oxidized after heat treatment. The Raman spectra in Figure 4f shows high quality multilayer graphene characteristics of the coated Cu/Ni foil revealed by a low D band in conjunction with the distinct G and 2D peak shapes. Bare Cu/Ni foil shows CuO (299, 342, 634 cm^{-1}) and Cu_2O (218 cm^{-1}) peaks as well as NiO peaks (550 and 1100 cm^{-1}) [141, 142].

This work opened the door of graphene research for thermal stability and oxidation resistance. It established a model and offered an orientation guiding the further deeply study. Based on this work, Kwon et al. [143] recently reported a new strategy to use graphene and metal-chloride-doped graphene (D-G) over layers for improving thermal stability, and they found that the thermal stability was effectively extended. Liang and co-workers [144] utilized a similar system, and they proved (by using electrochemical corrosion tests) that 7 min is the optimized growing time for protection against corrosion among all graphene coated Cu samples. Nguyen [145] reported the limit of graphene as a diffusion barrier is 800^{O}C.

Wetting transparency

As explained, graphene offers an unpenetrable barrier for external agents but, surprisingly, it also presents a more exotic property: wetting transparency. The chemical interaction between a graphene-coated material and environment is non-ignorable. In many applications the properties of coated materials need to be maintained. As a plain example, three dimensional coatings like paints [146], oxides [147], polymers [148], or metallic stacks [149], have shown to be a reliable coating for many applications, but the main drawback is that their three dimensional structure can alter the electrical, physical, thermal and chemical properties of the material underneath. On the contrary, due to its two dimensional nature, graphene can offer an efficient barrier without altering many of those properties. Rafiee et al. [17] investigated the impact of wettability to several materials, copper, gold, silicon and glass by coating the materials with graphene in different layers. They found that if the materials were coated by single layer graphene, the wettability of Cu, Au and Si had no apparent change. This phenomenon was defined as 'wetting transparency' which means the graphene sheet was 'indeed there' but seemed 'not there'. However, the wettability of glass was changed remarkably by the inserted graphene, which means graphene was not "wetting transparent" to glass.

As shown in Figure 5a, the water contact angles on naked Au and Si surface were 32.6^{O} and 77.4^{O}, respectively. After coated by a graphene monolayer, the corresponding contact angles were altered to 33.2^{O} and 78.8^{O}, respectively, resulting in only a ~1-2% increase. Similar phenomena were observed on Cu substrates: a graphene monolayer lead to a contact angle increase of only 0.7%, from 85.9^{O} to 86.2^{o} as shown in Figure 5b. Along with the graphene thickness increase, the contact angle continuously raised. Two and three layers did not

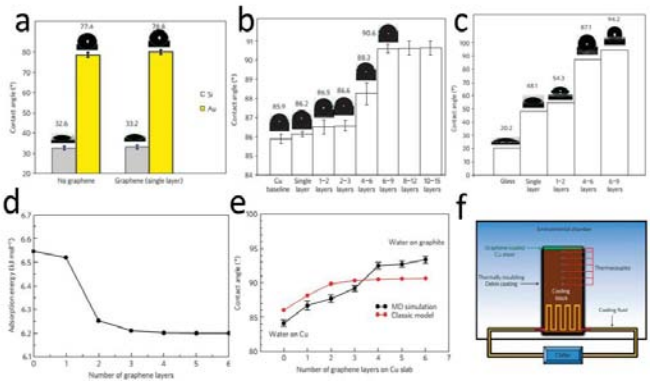

Figure 5: (a) Water contact angle measurements for Si and Au substrates with and without a monolayer graphene coating. Water contact-angle measurements on Cu (b) and glass (c) substrates with different numbers of graphene layers. (d) Predicted adsorption energy of water on Cu substrates with different numbers of graphene layers. (e) Comparison of the molecular-dynamics predictions with continuum predictions based on the classical effective-interface-potential approach. (f) Test set-up showing the graphene-coated Cu sheet mounted on a thermally insulated cooling block in an environmental chamber. An array of thermocouples are used to measure the temperature of the Cu sheet surface, the ambient temperature and the 1D heat flux through the cooling block. Reprinted with permission from Ref. [17]. Copyright ©2012 Nature Pub. Group.

introduce an apparent increase of contact angle (86.6^{O}), but when four layers were coated a sudden increase to 88.3^{O} was observed. The water contact angle finally saturated at the bulk graphite value (~90.6^{O}) for more than six graphene layers. In other words, monolayer graphene coatings offer wetting transparency to the underlying substrates like Cu, Au and Si. Differently, wetting transparency of graphene wasn't observed on glass surface where short-range chemical forces (hydrogen bonding with water) dominated the water contact angle. As shown in Figure 5c, naked glass had a contact angle of ~ 20.2^{O} and a coated graphene monolayer caused an apparent increase of contact angle to 48.1^{O}. The saturated contact angle was ~94^{O} after the coated graphene layers exceeding 6, which was also close to that of the bulk graphite value.

Water contact angle on a material surface is related to the absorption energy [150,151], and therefore, the wetting transparency of graphene on Cu can be understood in terms of how the graphene layer affects the adsorption energy of water on the Cu substrate. Water molecules interact with neighbouring Cu atoms within the interaction range when absorbed on the Cu substrate. Thus the inserted graphene monolayer just changes the topmost layer of Cu without any replacement of majority of the Cu neighbors. Figure 5d shows the predicted adsorption energy for Cu substrates with different numbers of graphene layers. It can be easily recognized that the adsorption energy of water on Cu can be differed only 0.4% by coating Cu substrate with graphene monolayer. The thinness geometry plays a main role on this wetting transparency because it doesn't influence the adsorption energy of water molecules with the substrate. The adsorption energy decrease is related to the increasing number of graphene layers and it reaches saturation at ~4 layers. Classical Young-Dupre equation [152-154] and their proposed molecular dynamics (MD) model were employed to compare the contact angles for water on Cu with different numbers of layers of graphene, as shown in Figure 5e. Both the models qualitatively reproduce the

contact-angle transition observed in the experiments (Figure 5d). The authors concluded that the wetting transparency of graphene is attributable to its extreme thinness because the relatively long-range van der Waals interaction (between water and Cu) dominates. It also provided an explanation why the wetting transparency breaks down for surfaces such as glass where chemistry plays the dominant role: the introduction of graphene at the water/glass interface will disrupt the short-range chemical interactions that play a dominant role in determining the water/glass contact angle.

Condensation heat transfer experiments on a Cu sheet (40 mm in diameter) with and without monolayer-graphene deposition were carried out to testing the function of graphene (Figure 5f). In this trial, surface oxides and strongly variation of surface wettability may introduce negative impacts, because oxides play the role of a thermal barrier that reduces the heat transfer coefficient at Cu interfaces. This phenomenon can turn the material surface into hydrophilic, which can lead to a liquid film which adversely affects condensation heat transfer [155]. The experiments demonstrated for the first time that the condensation heat transfer was enhanced by approximately 30-40% (over a wide range of temperatures) by coating Cu with graphene.

Understanding to graphene's wettability opened a new field for its applications. Specially, when oxygen-containing functional groups are introduced in the basal plane, graphene can be tuned hydrophilic [156]. Along with the increasing of the oxygen-containing functional group concentration, the water contact angle decreases. On the other hand, hydrophobic effect can be achieved by electrically doping of single layer graphene [157], which contributes to renormalization of the surface tension between graphene and water. In the same line, artificial superhydrophobic graphene was also reported [158]. By combining the wettability of graphene, not only wetting transparency can be carried out, but also slip flow inside the interlayer gallery between graphene layers can be optionally enhanced and broken down [159].

State-of-the-art of graphene as anti-corrosion layer

Graphene singer layer was recently reported to be successfully used as coating material to prevent oxidation of different underlying substrates [134]. As mentioned, the genuine sp^2 hexagonal distribution of carbon atoms provides an impermeable physical barrier that avoids substrate-environment interaction, as already demonstrated in other ultra-thin carbon-based structures such as carbon nanotubes [160]. Cho et al. and Chen et al. have demonstrated that graphene can provide effective oxidation resistance for the underlying Cu and Cu/Ni alloys [134,161] as we mentioned in last section. Prasai et al. and Kirkland et al. have demonstrated that graphene films could serve as corrosion-inhibiting coatings and have studied the passivation mechanism using electrochemical techniques [126,162] respectively, as described in the Section 2. Recently, Podila et al. have reported that graphene coating could enhance both bio- and hemo-compatibility of implant materials [163,164]. Notably, it has been found that almost all the cell viability results with the presence of graphene coated NiTi were similar or even lower than those observed for pristine NiTi, indicating a modest protection offered by graphene to NiTi [163,164]. Zhang et al. [165] performed the experiments studying the protection of Cu by graphene in live animals to evaluate its potential as a biocompatible passivated coating for metals in physiological conditions. His study reveals that graphene coating could be used as a possible versatile strategy to protect metals under physiological conditions, opening up the door for its biomedical application, such as metal implants. So the research on its oxidation resistance has diverse potential applications.

It has been demonstrated that the oxidation stability of graphene is strongly related to its nanostructure. Li et al. [166] designed a method to monitor the growth process of graphene on Cu or Ni substrate by alternately injection of ^{12}C and ^{13}C sources. He found that, on Ni substrate the dispersion of ^{12}C and ^{13}C was random but on Cu substrate it was regionally pure, that is, on Ni surface it was a 'segregation' and 'precipitation' process, but on Cu surface the formation process was driven by 'absorption'. But similarly, in both cases the so called 'wrinkles' appeared, which confined the domain size in several micrometers. These wrinkles were due to the different coefficient of thermal expansion between graphene/graphite and the underlying metal substrate [167,168]. Figure 6a shows an optical micrograph of the graphene film transferred onto a SiO_2/Si substrate from the original deposited Cu foil [50,169]. The Raman spectra in Figure 6b shows the graphene having regions close to pure ^{12}C (green), regions of isotopically pure ^{13}C (blue), and regions containing both ^{12}C and ^{13}C (red). The colors of Raman patterns are corresponding to the mark circles in Figure 6a. But, due to the unavoidable presence of defects, its degree of protection is also not ideal. Graphene flakes synthesized by any method always contain a certain degree of non-idealities, such as domain boundaries rich in pentagonal and

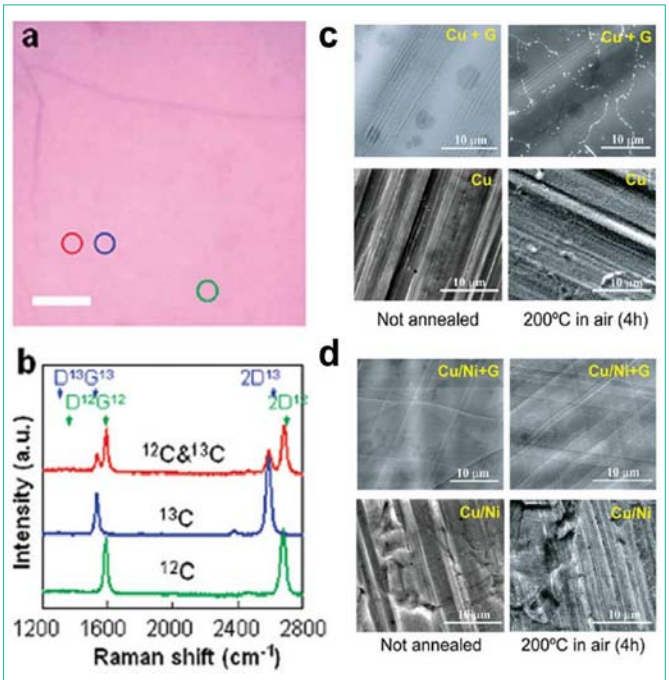

Figure 6: (a) An optical micrograph of the identical region analyzed with micro-Raman spectroscopy. (b) Raman spectra from ^{12}C-graphene (green circle), ^{13}C-graphene (blue circle), and the junction of ^{12}C- and ^{13}C-graphene (red circle), respectively. (c) SEM images of graphene coated (upper) and uncoated (lower) Cu foil taken before (left column) and after (right column) annealing in air. (d) SEM images of graphene coated (upper) and uncoated (lower) Cu/Ni foil taken before (left column) and after (right column) annealing in air. Reprinted with permission from Ref. [166,134]. Copyright 2009 American Chemical Society & 2011 American Chemical Society.

heptagonal lattices, missing bonds, impurities and wrinkles, leading to an inhomogeneous degree of protection. The first sign of non-ideality of graphene coating dates from 2009. In the same work in which the anti-oxidation property of graphene was reported [134], the authors suggested the local oxidation of the protected material can take place at the graphene defects, mainly located at the domain boundaries. More specifically, the SEM micrograph had a number of small bright white spots representing oxides formed (Figure 6c,d), most likely at the graphene grain boundaries or defect sites of the graphene surface [166]. Similarly, short time exposure to the oxidizing aqueous solution of H_2O_2 showed also significant attacked in few spots (white regions) after 15 and 5 min of H_2O_2 exposure, respectively.

The imperfections of graphene as anti-oxidation coating were further accentuated by Schriver [170] and the co-workers, who performed long-term research. They found that graphene could offer effective short-term oxidation protection, but it played a reverse role over long time scales, namely, it promoted more extensive wet corrosion than that seen for an initially bare, unprotected Cu surface. In their work they used two sets of samples, the first consisting on bare Cu foils and the other GSL/Cu stacks. As shown in Figure 7a and c, the as prepared bare Cu foils had the similar shiny appearances to the monolayer-graphene-coated samples. The colors of all samples were same and difficult to be distinguished by naked eyes. They analyzed two groups of samples, and in each group there was a bare

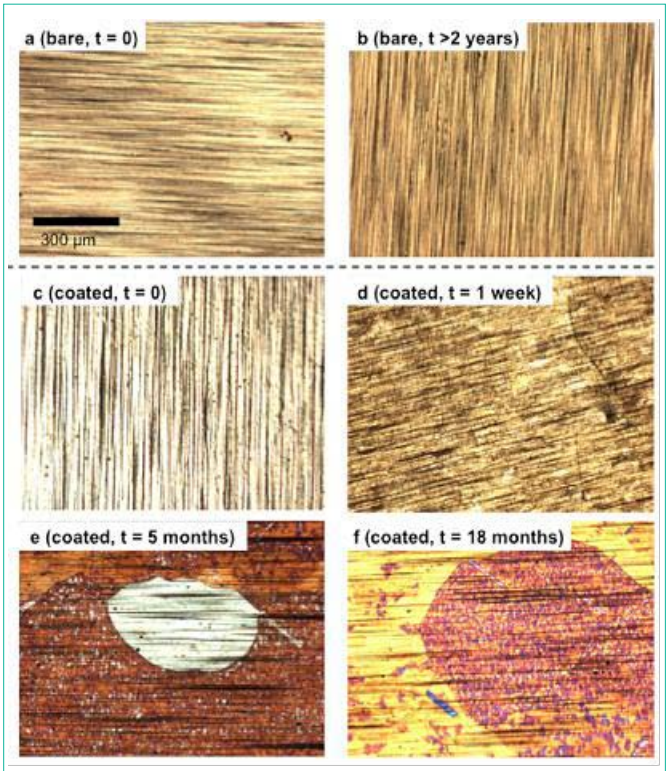

Figure 7: Optical micrographs of (a) as bare Cu, (b) bare Cu oxidized in ambient conditions over 2 years, (c) as prepared graphene-coated Cu, (d) graphene-covered Cu 1 week after graphene growth, (e) graphene-covered Cu 5 months after graphene growth and (f) graphene-covered Cu 18 months after graphene growth. All the samples were put in ambient conditions. Reprinted with permission from Ref. [170]. Copyright 2013 American Chemical Society.

Cu foil and a monolayer-graphene-coated one. The two groups were treated in ambient at 250°C and 185°C, respectively. At 250°C, 6 min was long enough to make the bare Cu significantly oxidized, while the graphene-coated Cu sample showed little oxidation. Despite these initial promising results, a 17-hour heat treatment revealed that under such conditions both the bare and graphene-coated Cu foils were heavily oxidized and indistinguishable. This surprise was not an accidental phenomenon, the similar process occurred at 185°C. At 185°C, after 15 min the bare Cu was partially oxidized, while the monolayer-coated Cu was close to its pristine state. After 17 h in air at 185°C, both the bare Cu and the monolayer-graphene-coated Cu were heavily oxidized, as to their counterparts at 250°C. The difference is that the effective time scale for thermal oxidation protection by graphene on Cu is on the order of 1 h at 185°C, about an order of magnitude longer than similar systems at 250°C. These two cases are consistent to other recent reports [126,134,162,171,172], in which graphene provides significant short-term thermal oxidation protection to Cu at very high temperatures and short times (several minutes). It is concluded that graphene serves as an impressive oxidation barrier for Cu, likely due to the low permeability of graphene to gases, but at a long time scale the graphene-coated Cu succumbs to thermal oxidation, as corroborated by Raman spectroscopy. Even longer time analyses revealed further interesting information: i) oxidation of graphene-coated Cu initially occurs in the relatively sparse regions of graphene grain boundaries, cracks, and point defects. ii) The longest time scale for graphene protecting Cu from oxidation or corrosion is weeks (Figure 7d). Over longer time scales at room temperature, the Cu surface was uniformly oxidized (Figure 7e and f), much worse compared to the bare Cu substrate (Figure 7b). It seems that graphene even promoted Cu corrosion instead of preventing it. From an extended-duration experiment carried out at 25°C up to 18 months it was found the Cu substrate covered with monolayer graphene was even more heavily oxidized than the same sample treated at 250°C for 17 hours, with a production of Cu_2O, rather than CuO. Thus, at room temperature and in time scales over 1 month, graphene plays the role for long-term metal oxidation barrier. Three aspects were thought responsible for the worse performance of graphene on long-term oxidation resistance. Firstly, highly conductive graphene and Cu drive galvanic corrosion of Cu [172,173] by maintaining charge transfer to the bulk of the Cu, and allowing the full electrochemical reaction to continue unimpeded because the graphene coating maintains electrical contact across the surface of the Cu and sparse protected regions of Cu. Secondly, over several months O_2 and H_2O infiltrate and bleed through the defects in the graphene, diffusing between the graphene and Cu, oxidizing or corroding the entire surface of the underlying substrate. Additionally, non-uniform oxidation beginning at graphene defects lead to stress and cracking of the oxide layer, which opens up new avenues for corrosion. From the geometric point of view, a solution to deal with this problem is taking bilayer graphene as a succedaneum to replace graphene monolayer, since the defects of both layers will rarely coincide at the same location.

Ageing of Graphene-coated Materials

The intrinsic inhomogeneities of graphene lead to a diversity of surface defects that act differently in contact with the environment (gas and liquids). Therefore, the introduction of graphene in

real applications requires an exhaustive characterization of these features, including reliability models and lifetime predictions. It seems evident that the modifications produced on graphene-coated metals are related to local oxidation. In our previous work [174], we demonstrate that local oxidation of graphene-coated materials can effectively happen, and it can dramatically modify the performance of real devices. Therefore, the ageing of graphene-coated materials should be studied in each specific application to be able to make lifetime predictions.

Figures 8a and 8b show the simultaneously collected topographic and current images of the sample treated in H_2O_2 for one hour. Both figures show important inhomogeneities, due to the formation of a network of hillocks at the graphene surface during the treatment. At the locations where hillocks were formed the conductivity was dramatically reduced. The same phenomenon was also observed when oxidizing the samples in air. The Auger Electron Spectroscopy (AES) oxygen maps (Figure 8c) reveal that plateaus and hillocks show different amounts of oxygen, and the patterns of oxygen signal are apparently similar to that of the bright spots in the SEM image (inset in Figure 8c). It is worth noting that the hillocks outline regions with shapes and sizes similar to the graphene domains. Pentagonal and heptagonal defects originated from the missing bonds at the GSL domain boundaries may be responsible to the inhomogeneous oxidation.

Wei et al. further explored this phenomenon by utilizing the molecular dynamics (MD) simulations and continuum mechanics [175]. It was well known that at the atomic level, boundaries in graphene are usually formed by typical defects of pentagon-heptagon rings [176-180], but these features are not uniformly spaced and their accumulation leads to the non-uniformity of graphene in terms of forming tilt boundaries, namely armchair tilt boundaries and zigzag tilt boundaries. In general, increasing tilt angles can introduce more boundary defects, leading to higher boundary energy. Armchair tilt boundaries under present consideration are either composed of an array of uniformly distributed disclination dipoles (Figure 8d) or an array of disclination dipole clusters (Figure 8f, h). MD simulations for calculation of the stress contours are shown in Figure 8e, g, i, respectively, for the corresponding boundaries shown in Figure 8d, f and h. For the stress induced by disclination clusters (Figure 8f, h), it was found that the top-most dipole in a cluster has the highest normal stress (Figure 8g, i). In comparison, zigzag tilt boundaries were formed by evenly spaced disclination clusters, as shown in Figure 8j, where the stress induced by the disclination clusters (Figure 8k) is much greater than that by the disclination dipole in Figure 8e. The stress can be sorted as zigzag tilt boundaries - armchair tilt boundaries - domains, and the energy for each situation is ranked in the same. So the zigzag tilt boundaries are most sensitive to the environment variations, followed by the armchair tilt boundaries. The combination of zigzag tilt boundaries and armchair tilt boundaries causes the formation of defect boundaries of graphene. This also explains why the oxidation preferentially happens at the corners of the domain boundaries than along with the boundaries. The results are consistent with the observation mentioned in Figures 6c and d.

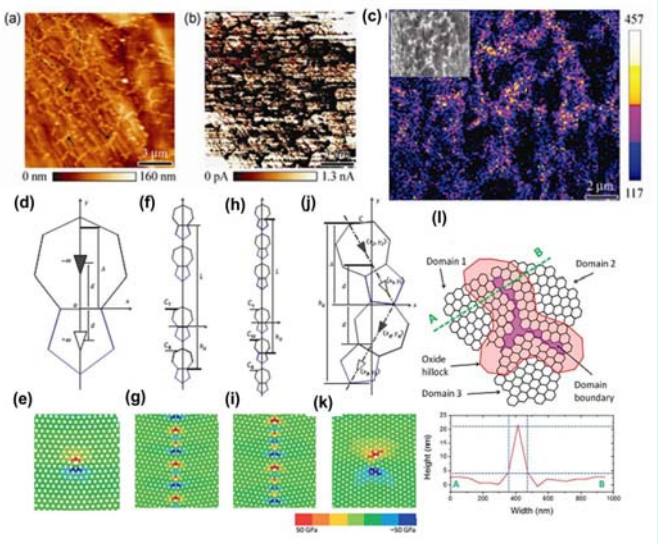

Figure 8: (a) topographic and (b) current maps when scanning the surface of a GSL/Cu sample that was soaked in H_2O_2 for 1 h. (c) The content of oxygen map measured with AES on the GSL/Cu sample soaked in H_2O_2 for 1 h. (inset) corresponding to SEM image of the same location. (d) A disclination dipole formed by a pentagon–heptagon defect. (f, h) Armchair tilt boundaries with tilt angles θ=16.4° and θ=17.9° formed by evenly displaced disclination clusters. (j) Disclination clusters in zigzag tilt boundaries. (e, g, i, k) Normal stress contours induced by defects from (d, f, h) and (j), respectively. (l) Schematic of the formation and propagation of the oxide hillock around the domain boundary and the lower curve shows the statistical analyses of width and height of the hillocks. Reprinted with permission from Ref. [174,175,181]. Copyright ©2013, Tsinghua University Pressand Springer-Verlag Berlin Heidelberg & 2012 Nature Publishing Group.

We observed such boundaries after full oxidized in H_2O_2 for 1 h [181] and statistically showed that the boundaries were ~215 nm in width and ~10 nm in height at the saturated state. Figure 8 shows a schematic of one oxidized region of an 8.4 μm x 14.4 μm area. A calculation was made using a threshold slightly and the mean value of the area covered by the oxidation paths was 23.61%. The graph below shows one example of a real cross section in a region similar to the A-B line in the schematic. In this work, we also observed the formation and propagation of the oxide hillock around the domain boundaries. Initially, no corrugations have been observed. Soon, we observed some areas with narrow and low density hillocks while others kept unaltered. Finally, the hillocks with high density became wider and show the network on the whole area. Interestingly, we observed that the graphene sheets exposed to H_2O_2, in which the accumulation of oxygen at the graphene domain boundaries evolves in a very controlled and progressive way. Furthermore, the oxide hillocks can propagate with the soaking time until reaching a limit width and height, which can drastically reduce the performance of a whole graphene sheet. All these results conform to the applied simulation.

To lower the ageing effect of graphene, on one hand the material quality itself should be steady improved, and on the other, new designs are needed to protect the utilized graphene. From the material point of view, graphene should be synthesized with few defects and in a large scale. Some of the techniques described in introduction section tried to fulfill this requirement, and every day we see more and more reports in this direction. Wu et al. [182] reported the synthesis of graphene by employing hydrogen arc discharge. Using this method graphene defects could be in situ healed by high plasma temperature and etching effect of H_2 on amorphous carbon [183,184]. By this

method, H2 is added in, and the oxygen-containing groups tend to be removed in the form of H_2O instead of CO_2, avoiding the production of vacancies (lower loss of carbon atoms). The thus formed graphene possesses superior advantages, such as good crystallinity, high thermal stability and high electrical conductivity (~2×10^3 S/cm). Strong et al. [185] developed an inexpensive process to deoxygenate graphite oxide layers to create laser scribed graphene (LSG) by using laser. The LSG can be directly patterned onto various flexible substrates without masks, templates, post-processing, transferring techniques, or metal catalysts. The electrical conductivity of LSG is tunable over 5 orders of magnitude by varying the laser intensity and laser irradiation treatments. Lee and co-workers [186] recently reported a new scheme to synthesize graphene on the surface of hydrogen-terminated germanium buffer layer on silicon. The prepared graphene was wrinkle-free single-crystal monolayer in wafer-scale. The germanium (110) surface offers unidirectional alignment conditions by its anisotropic two fold symmetry, causing single-crystal graphene growth with predefined orientation. Importantly, carbon atoms in the graphene were fully sp^2-hybridized without a bonding interaction with the underlying Ge surface, which enabled the facile etch-free dry transfer of graphene and the recycling of the germanium substrate for continual graphene growth.

As discussed above, graphene is also oxidized, which might limit its applications. Actually, all carbon materials, like carbon nanotubes and graphene, are not absolutely stable as their ends or edges are readily oxidized owing to the presence of more defects, such as dangling bonds in regions that are susceptible to be attacked by OH– ions [187] as shown in Figure 9. Li et al. [188] reported that the double layer capacitance (DLC) of nanographite materials (NGMs) before oxidation reaction is directly proportional to the level of oxidation of the NGMs in the electrolyte, with large DLC leading to poorer oxidation stability for the NGMs. They introduced a perfluorosulfonic acid (PFSA) polymer to selectively modify the surface of the NGMs (PFSA-NGMs) and reduce the DLC by diminishing the electric conductivity and limiting adsorption of electrolyte ions on the surface of NGMs. The results showed that the DLC of PFSA-graphene dropped to 66% of the original graphene, proving the effectiveness of the polymer functionalization to prevent oxidation of NGMs by decreasing their DLC. Another methodology to develop protective coatings is to combine graphene with other nanostructured materials, like carbon nanotube and metal nanowires [25-27]. It was proved that hydrazine-reduced graphene combined with carbon nanotubes has the potential to be used as a transparent conductor alternative to indium tin oxide (ITO). An ingenious design was proposed by Lee et al. [189] using two-dimensional graphene and one-dimensional NWs in a hybrid film, leading to flexible and stretchable, transparent electrodes. Using such methodology, electrical properties were significantly enhanced with negligible degradation of optical transmittance. The hybrid electrode presents superb mechanical flexibility and stretch ability, which enables complete folding in half. Interestingly, the fabricated electrodes were used in an inorganic light-emitting diode (ILED, Figure 10a), which was attached to an eye contact lens (Figure 10b). After rubbing this ILED on the eye of a mannequin (Figure 10c) or in a live rabbit eye for five hours (Figure 10d) it was still working with emitting light (Figure 10e) without any abnormal behavior of the live rabbit like bloodshot eyes. The turn-on voltage was maintained after this in-vivo experiment with a negligible resistance increase. Such performance is related to the slight slipping of ILED on the surface of

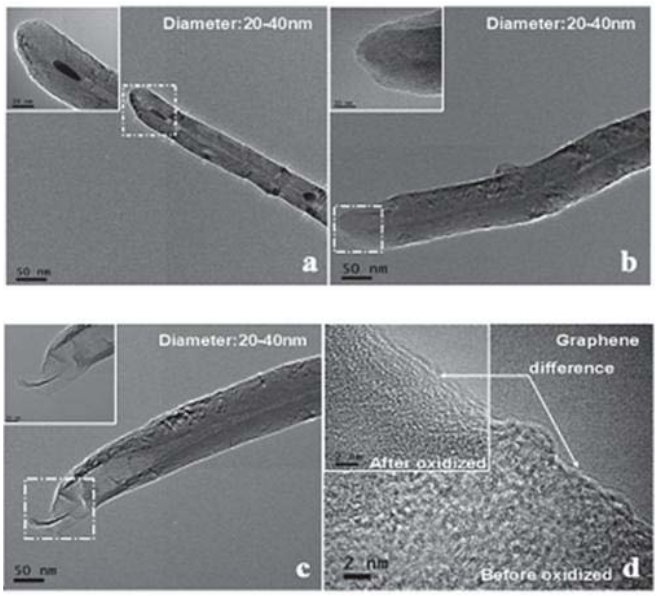

Figure 9: TEM images of CNT2040 (inset: enlarged images) (a) before and after oxidation of (b) 30-minutes and, (c) 48-hours. (d) TEM image of graphene before and after (inset) oxidation. Reproduced with permission from Ref [188]. Copyright© 2013 WILEY-VCH Verlag GmbH & Co. KGaA, Weinheim.

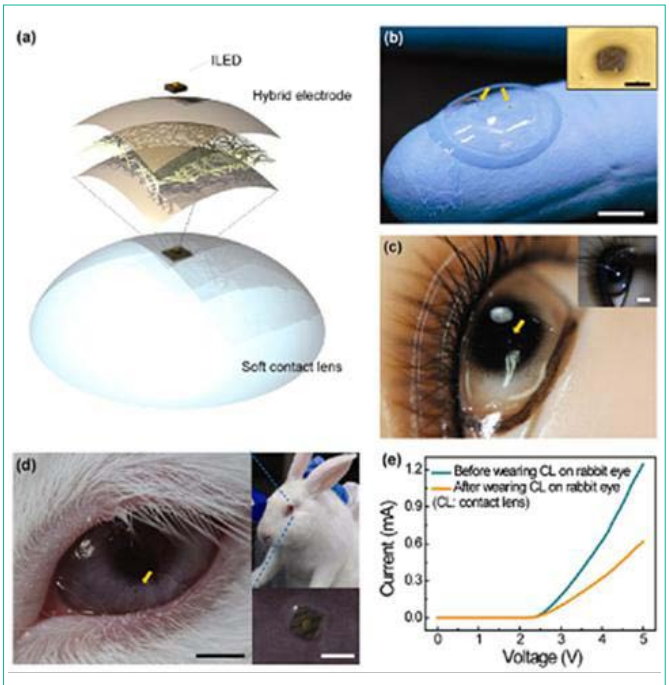

Figure 10: (a) Schematic illustration of the single-pixel contact lens display layout. The photograph of (b) the contact lens device (Inset: optical microscopic image of slightly sunken ILED on the surface of hybrid electrode and contact lens) and (c) the ILED-hybrid electrode-contact lens device on an eye of a mannequin (Inset: a photograph for emitting light of contact lens device on a mannequin eye after supplying bias.). (d) The photograph of contact lens device on a rabbit eye and magnified image of ILED part of the device (right-bottom inset). (e) I–V characteristic curve of ILED before and after wearing contact lens device on a rabbit eye. Reprinted with permission from Ref. [189]. Copyright 2013 American Chemical Society.

the hybrid electrode by the regular eye nictation of the live rabbit. It is a new tendency to develop biocompatible and conductive adhesives, fabricate multiple pixel displays on wearable contact lenses for next generation of future displays.

Prospect

Graphene and other carbon-based materials (such as carbon nanotubes) have shown that its pristine structure can lead to a wide branch of genuine properties, which have been intelligently used by the scientific community to report a huge amount of prototypes. Now the challenge is to shift from laboratory prototypes to commercial products for the society. The good news are that, after a decade working with graphene, now the properties of graphene are well described, which creates a suitable landscape for engineers to start including graphene in new-concept devices. So it is believable that the potential of graphene has just been started to be explored, and transferring graphene capabilities to the market is one of the main global goals for the next ten years. As an example, the European commission has invested 1 billion of Euros in a framework program dedicated to graphene-based technologies (http://europa.eu/rapid/press-release_MEMO-14-316_en.htm), and big corporations like IBM, Samsung and Sandisk, are influential in the entire graphene production chains. BCC Research released a new edition to their "Graphene: Technologies, Applications and Markets" report. They forecast that the global graphene product market will reach $195 million in 2018. This will grow quickly to $1.3 billion by 2023 (an annual growth rate of 47.1%) [71].

In the field of using graphene as protective coating, the key factor defining its performance is the sheet quality. The main factor that reduces the performance of graphene is its amount of defects. The most common non-idealities in graphene sheets are: i) missing bonds, ii) pentagonal and hexagonal lattices, iii) lattice distortions, iv) local thickness fluctuations, and v) doping with impurities. All these factors can, not only alter the properties of graphene, but when using it as protective coating they can represent centers for damage accumulation. As explained in sections 3, 4 and 5, local defects in graphene can lead to accumulation of oxygen, which impoverishes the mechanical, electronic and chemical properties of the sheet. On the contrary, the pristine hexagonal structure of graphene conform a perfect impermeable barrier for material protection. Undoubtedly, the material still needs to be ameliorated in the sense of defects confinement, and therefore, the future improvement of graphene coatings seems to be linked to the reduction of defects. One of the main targets is to minimize the amount of graphene domain boundaries, since they contain most of defects. Moreover, using selective substrates to grow the material by CVD and that minimize the introduction of impurities in the carbon lattice is also highly desirable. Finally, the production of large area sheets is one of the main requirements for its use as protective coating (and it plays a more important role compared to microelectronic applications), since the areas to be protected are normally at the macroscopic scale.

Conclusion

In this review, we have highlighted several novel applications of graphene based electrodes, specially focusing on its use as protective coating. Graphene as anti-corrosion coating is very attractive because it may protect many metals by keeping unaltered their intrinsic properties, which is something cannot be achieved using three dimensional protective paints, oxides or polymers. Moreover, the use of graphene in this field doesn't require device patterning, which could decrease the quality of the two dimensional sheet. But the problem is that the graphene sheets synthesized using the current methods still contain too many defects, which can lead to an imperfect protection degree, especially in long-term experiments. Therefore, the ageing of graphene intrinsic properties and the reliability tests of graphene-based prototypes is an essential step prior to their introduction in the industry, and many engineers and scientists will have to face it in the next years.

Acknowledgements

Mario Lanza acknowledges generous startup funding from Soochow University. Huiling Duan would like to acknowledge the Alexander von Humboldt (AvH) foundation in Germany to support this work through project "Mechanics theory of materials with complex surfaces and its applications" in the frame of the AvH program for funding a research group linkage.

References

1. Peierls R. Remarks on the Theory of Metals. Z Phys. 1934; 88: 786-791.
2. Peierls R. On the Statistical Basis for the Electron Theory of Metals. Helv Phys Acta. 1934; 7: 24-30.
3. Peierls R. Remarks on Transition Temperatures. Helv Phys Acta. 1934; 7: 81-83.
4. Mermin N, Wagner H. Absence of Ferromagnetism or Antiferromagnetism in One- or Two-Dimensional Isotropic Heisenberg Models. Phys Rev Lett. 1966; 17: 1307.
5. Novoselov KS, Geim AK, Morozov SV, Jiang D, Zhang Y, Dubonos SV, et al. Electric field effect in atomically thin carbon films. Science. 2004; 306: 666-669.
6. Geim AK. Graphene: status and prospects. Science. 2009; 324: 1530-1534.
7. Wu J, Pisula W, Müllen K. Graphenes as potential material for electronics. Chem Rev. 2007; 107: 718-747.
8. Rao C, Sood A, Voggu R, Subrahmanyam K. Some Novel Attributes of Graphene. J Phys Chem Lett. 2010; 1: 572-580.
9. Allen MJ, Tung VC, Kaner RB. Honeycomb carbon: a review of graphene. Chem Rev. 2010; 110: 132-145.
10. Lee C, Wei X, Kysar JW, Hone J. Measurement of the elastic properties and intrinsic strength of monolayer graphene. Science. 2008; 321: 385-388.
11. van den Brink J. Graphene: from strength to strength. Nat Nanotechnol. 2007; 2: 199-201.
12. Balandin AA, Ghosh S, Bao W, Calizo I, Teweldebrhan D, Miao F. Superior thermal conductivity of single-layer graphene. Nano Lett. 2008; 8: 902-907.
13. Schadler S, Giannris C, Ajayan P. Load Transfer in Carbon Nanotube Epoxy Composites. Appl Phys Lett. 1998; 73: 3842-3847.
14. Zhang Y, Tan YW, Stormer HL, Kim P. Experimental observation of the quantum Hall effect and Berry's phase in graphene. Nature. 2005; 438: 201-204.
15. Mayorov AS, Gorbachev RV, Morozov SV, Britnell L, Jalil R, Ponomarenko LA, et al. Micrometer-scale ballistic transport in encapsulated graphene at room temperature. Nano Lett. 2011; 11: 2396-2399.
16. Nair RR, Blake P, Grigorenko AN, Novoselov KS, Booth TJ, Stauber T, et al. Fine structure constant defines visual transparency of graphene. Science. 2008; 320: 1308.
17. Rafiee J, Mi X, Gullapalli H, Thomas AV, Yavari F, Shi Y. Wetting

transparency of graphene. Nat Mater. 2012; 11: 217-222.

18. Service RF. Materials science. Carbon sheets an atom thick give rise to graphene dreams. Science. 2009; 324: 875-877.

19. Weitz RT, Yacoby A. Nanomaterials: Graphene rests easy. Nat Nanotechnol. 2010; 5: 699-700.

20. Jeon I, Choi H, Bae S, Chang D, Baek J. Wedging Graphite into Graphene and Graphene-like Platelets by Dendritic Macromolecules. J Mater Chem. 2011; 21: 7820-7826.

21. Pereira V, Castro Neto A, Peres N. Tight-Binding Approach to Uniaxial Strain in Graphene. Phys Rev B. 2009; 80: 045401.

22. Liao L, Bai J, Lin YC, Qu Y, Huang Y, Duan X, et al. High-performance top-gated graphene-nanoribbon transistors using zirconium oxide nanowires as high-dielectric-constant gate dielectrics. Adv Mater. 2010; 22: 1941-1945.

23. Stankovich S, Dikin DA, Dommett GH, Kohlhaas KM, Zimney EJ, Stach EA, et al. Graphene-based composite materials. Nature. 2006; 442: 282-286.

24. Bunch JS, Verbridge SS, Alden JS, van der Zande AM, Parpia JM, Craighead HG, et al. Impermeable atomic membranes from graphene sheets. Nano Lett. 2008; 8: 2458-2462.

25. Tung VC, Chen LM, Allen MJ, Wassei JK, Nelson K, Kaner RB, et al. Low-temperature solution processing of graphene-carbon nanotube hybrid materials for high-performance transparent conductors. Nano Lett. 2009; 9: 1949-1955.

26. Wassei J, Kaner R. Graphene, a Promising Transparent Conductor. Mater Today. 2010; 13: 52-59.

27. Hecht D, Kaner R. Solution-Processed Transparent Electrodes. MRS Bull. 2011; 36: 749-755.

28. Chae HK, Siberio-Pérez DY, Kim J, Go Y, Eddaoudi M, Matzger AJ, et al. A route to high surface area, porosity and inclusion of large molecules in crystals. Nature. 2004; 427: 523-527.

29. Viculis LM, Mack JJ, Kaner RB. A chemical route to carbon nanoscrolls. Science. 2003; 299: 1361.

30. Stoller MD, Park S, Zhu Y, An J, Ruoff RS. Graphene-based ultracapacitors. Nano Lett. 2008; 8: 3498-3502.

31. Stefan B, Hendrik V, Karsten H. Reversible Photon-induced Oxidation of Graphene by NO2 Adsorption. Surf Sci. 2014; 621: 117-122.

32. Hoa L, Tien H, Luan V, Chung J, Hur S. Fabrication of a Novel 2D-graphene/2D-NiO Nanosheet-based Hybrid Nanostructure and Its Use in Highly Sensitive NO2 Sensors. Sensor Actuat B-Chem. 2013; 185: 701-705.

33. Inaba A, Yoo K, Takei Y, Matsumoto K, Shimoyama I. Ammonia Gas Sensing Using a Graphene Field-Effect Transistor Gated by Ionic Liquid. Sensor Actuat B-Chem. 2014; 195: 15-21.

34. Huang B, Li Z, Liu Z, Zhou G, Hao S, Wu J, et al. Adsorption of Gas Molecules on Graphene Nanoribbons and Its Implication for Nanoscale Molecule Sensor. J Phys Chem C. 2008; 112: 13442-13446.

35. Xu K, Meshik X, Nichols BM, Zakar E, Dutta M, Stroscio MA, et al. Graphene- and aptamer-based electrochemical biosensor. Nanotechnology. 2014; 25: 205501.

36. Yu D. Adsorption of Potassium on Graphite: Work Function Calculations. Tech Phys Lett. 2009; 35: 847-849.

37. Sofo J, Chaudhari A, Barber G. Graphane: A Two-Dimensional Hydrocarbon. Phys Rev B. 2007; 75: 153401.

38. Liu L, Shen Z, Liang S, Yi M, Zhang X, Ma S. Enhanced Atomic Oxygen Erosion Resistance and Mechanical Properties of Graphene/Cellulose Acetate Composite Films. J Appl Polym Sci. 2014; 131: 40292.

39. Fujii S, Enoki T. Cutting of oxidized graphene into nanosized pieces. J Am Chem Soc. 2010; 132: 10034-10041.

40. Ong MT, Reed EJ. Engineered piezoelectricity in graphene. ACS Nano. 2012; 6: 1387-1394.

41. Li X, Kong F, Liu J, Liang T, Xu J, Chen H. Synthesis of Potassium-Modified Graphene and Its Application in Nitrite-Selective Sensing. Adv Funct Mater. 2012; 22: 1981-1988.

42. Berger C, Song Z, Li X, Wu X, Brown N, Naud C, et al. Electronic confinement and coherence in patterned epitaxial graphene. Science. 2006; 312: 1191-1196.

43. Emtsev KV, Bostwick A, Horn K, Jobst J, Kellogg GL, Ley L, et al. Towards wafer-size graphene layers by atmospheric pressure graphitization of silicon carbide. Nat Mater. 2009; 8: 203-207.

44. Marchini S, Gunther S, Wintterlin J. Scanning Tunneling Microscopy of Graphene on Ru(0001). Phys Rev B. 2007; 76: 075429.

45. Loginova E, Bartelt N, Feibelman P, McCarty K. Evidence for Graphene Growth by C Cluster Attachment. New J Phys. 2008; 10: 093026.

46. Sutter PW, Flege JI, Sutter EA. Epitaxial graphene on ruthenium. Nat Mater. 2008; 7: 406-411.

47. Yu Q, Lian J, Siriponglert S, Li H, Chen Y, Pei S. Graphene Segregated on Ni Surfaces and Transferred to Insulators. Appl Phys Lett. 2008; 93: 113103.

48. Reina A, Jia X, Ho J, Nezich D, Son H, Bulovic V, et al. Large area, few-layer graphene films on arbitrary substrates by chemical vapor deposition. Nano Lett. 2009; 9: 30-35.

49. Kim KS, Zhao Y, Jang H, Lee SY, Kim JM, Kim KS, et al. Large-scale pattern growth of graphene films for stretchable transparent electrodes. Nature. 2009; 457: 706-710.

50. Li X, Cai W, An J, Kim S, Nah J, Yang D. Large-area synthesis of high-quality and uniform graphene films on copper foils. Science. 2009; 324: 1312-1314.

51. Blake P, Brimicombe PD, Nair RR, Booth TJ, Jiang D, Schedin F, et al. Graphene-based liquid crystal device. Nano Lett. 2008; 8: 1704-1708.

52. Jiao L, Zhang L, Wang X, Diankov G, Dai H. Narrow graphene nanoribbons from carbon nanotubes. Nature. 2009; 458: 877-880.

53. Cai J, Ruffieux P, Jaafar R, Bieri M, Braun T, Blankenburg S, et al. Atomically precise bottom-up fabrication of graphene nanoribbons. Nature. 2010; 466: 470-473.

54. Li X, Magnuson CW, Venugopal A, Tromp RM, Hannon JB, Vogel EM, et al. Large-area graphene single crystals grown by low-pressure chemical vapor deposition of methane on copper. J Am Chem Soc. 2011; 133: 2816-2819.

55. Qi M, Ren Z, Jiao Y, Zhou Y, Xu X, Li W, et al. Hydrogen Kinetics on Scalable Graphene Growth by Atmospheric Pressure Chemical Vapor Deposition with Acetylene. J Phys Chem C. 2013; 117: 14348-14353.

56. Guermoune A, Chari T, Popescu F, Sabri S, Guillemette J, Skulason H, et al. Chemical Vapor Deposition Synthesis of Graphene on Copper with Methanol, Ethanol, and Propanol Precursors. Carbon. 2011; 49: 4204-4210.

57. Choi JH, Li Z, Cui P, Fan X, Zhang H, Zeng C, et al. Drastic reduction in the growth temperature of graphene on copper via enhanced London dispersion force. Sci Rep. 2013; 3: 1925.

58. Wang Z, Han Q, Xia J, Xia L, Ding M, Tang J, et al. Graphene-based solid-phase extraction disk for fast separation and preconcentration of trace polycyclic aromatic hydrocarbons from environmental water samples. J Sep Sci. 2013; 36: 1834-1842.

59. Li X, Cai W, Jung I, An J, Yang D, Velamakanni A, et al. Synthesis, Characterization, and Properties of Large-Area Graphene Films. ECS Trans. 2009; 19: 41-52.

60. Coraux J, N'Diaye AT, Busse C, Michely T. Structural coherency of graphene on Ir(111). Nano Lett. 2008; 8: 565-570.

61. Cai W, Zhu Y, Li X, Piner R, Ruoff R. Large Area Few-Layer Graphene/Graphite Films as Transparent Thin Conducting Electrodes. Appl Phys Lett. 2009; 95: 123115.

62. Fujita T, Kobayashi W, Oshima C. Novel Structures of Carbon Layers on a

Pt(111) Surface. Surf Interface Anal. 2005; 37: 120-123.

63. He Q, Sudibya HG, Yin Z, Wu S, Li H, Boey F, et al. Centimeter-long and large-scale micropatterns of reduced graphene oxide films: fabrication and sensing applications. ACS Nano. 2010; 4: 3201-3208.

64. Martins LG, Song Y, Zeng T, Dresselhaus MS, Kong J, Araujo PT, et al. Direct transfer of graphene onto flexible substrates. Proc Natl Acad Sci U S A. 2013; 110: 17762-17767.

65. Wang G, Zhang M, Zhu Y, Ding G, Jiang D, Guo Q, et al. Direct growth of graphene film on germanium substrate. Sci Rep. 2013; 3: 2465.

66. Dikin DA, Stankovich S, Zimney EJ, Piner RD, Dommett GH, Evmenenko G, et al. Preparation and characterization of graphene oxide paper. Nature. 2007; 448: 457-460.

67. Staudenmaier L. Verfahren zur Darstellung der Graphits Ure. Ber Dtsch Sch Chem Ges. 1898; 31:1481-1487.

68. Brodie B. Sur le Poids Atomique du Graphite. Ann Chim Phys. 1860; 59: 466-472.

69. Hummers W, Offeman R. Preparation of Graphitic Oxide. J Am Chem Soc. 1958; 80: 1339.

70. Tsuyoshi N, Yoshiaki M. Formation Process and Structure of Graphite Oxide. Carbon.1994; 32: 469-475.

71. Allied Market Research: the graphene material market will reach $149.9 million by 2020.

72. Lin Y, Chiu H, Keith A, Jenkins, Damon B, Farmer, et al. Dual-Gate Graphene FETs with f(T) of 50 GHz. IEEE Electron Device Lett. 2010; 31: 68-70.

73. Lin YM, Dimitrakopoulos C, Jenkins KA, Farmer DB, Chiu HY, Grill A, et al. 100-GHz transistors from wafer-scale epitaxial graphene. Science. 2010; 327: 662.

74. Farmer DB, Chiu HY, Lin YM, Jenkins KA, Xia F, Avouris P, et al. Utilization of a buffered dielectric to achieve high field-effect carrier mobility in graphene transistors. Nano Lett. 2009; 9: 4474-4478.

75. Jeon D, Lee K, Kim M, Kim D, Chung H, Woo Y, et al. Radio-Frequency Electrical Characteristics of Single Layer Graphene. Jpn J Appl Phys. 2009; 48: 091601.

76. Lin YM1, Jenkins KA, Valdes-Garcia A, Small JP, Farmer DB, Avouris P. Operation of graphene transistors at gigahertz frequencies. Nano Lett. 2009; 9: 422-426.

77. Moon JS. Epitaxial-Graphene RF Field-Effect Transistors on Si-Face 6H-SiC Substrates. IEEE Electron Device Lett. 2009; 30: 650-652.

78. Han SJ, Jenkins KA, Valdes Garcia A, Franklin AD, Bol AA, Haensch W, et al. High-frequency graphene voltage amplifier. Nano Lett. 2011; 11: 3690-3693.

79. Liao L, Lin YC, Bao M, Cheng R, Bai J, Liu Y, et al. High-speed graphene transistors with a self-aligned nanowire gate. Nature. 2010; 467: 305-308.

80. Aricò AS, Bruce P, Scrosati B, Tarascon JM, van Schalkwijk W. Nanostructured materials for advanced energy conversion and storage devices. Nat Mater. 2005; 4: 366-377.

81. Simon P, Gogotsi Y. Materials for electrochemical capacitors. Nat Mater. 2008; 7: 845-854.

82. Shaijumon MM, Ou FS, Ci L, Ajayan PM. Synthesis of hybrid nanowire arrays and their application as high power supercapacitor electrodes. Chem Commun (Camb). 2008; 2373-2375.

83. Yoon BJ, Jeong SH, Lee KH, Kim HS, Park CG, Han JH. Electrical Properties of Electrical Double Layer Capacitors with Integrated Carbon Nanotube Electrodes. Chem. Phys. Lett. 2004; 388: 170-174.

84. Wang Y, Shi Z, Huang Y, Ma Y, Wang C, Chen M, et al. Supercapacitor Devices Based on Graphene Materials. J Phys Chem C. 2009; 113: 13103-13107.

85. Du CS, Yeh J, Pan N. High Power Density Supercapacitors Using Locally Aligned Carbon Nanotube Electrodes. Nanotechnology. 2005; 16: 350.

86. Zhu Y, Murali S, Cai W, Li X, Suk JW, Potts JR, et al. Graphene and graphene oxide: synthesis, properties, and applications. Adv Mater. 2010; 22: 3906-3924.

87. Goler S, Coletti C, Piazza V, Pingue P, Colangelo F, Pellegrini V, et al. Revealing the Atomic Structure of the Buffer Layer between SiC(0001) and Epitaxial Graphene. Carbon. 2013; 51: 249-254.

88. Wang Z, Philippe L, Elias J. Deflection of Suspended Graphene by a Transverse Electric Field. Phys Rev Lett. 2010; 81: 155405.

89. Bae S, Kim H, Lee Y, Xu X, Park JS, Zheng Y, et al. Roll-to-roll production of 30-inch graphene films for transparent electrodes. Nat Nanotechnol. 2010; 5: 574-578.

90. Torrisi F, Hasan T, Wu W, Sun Z, Lombardo A, Kulmala TS. Inkjet-printed graphene electronics. ACS Nano. 2012; 6: 2992-3006.

91. Su CY, Xu YP, Zhang W, Zhao JW, Tang XH, Tsai CH, et al. Electrical and Spectroscopic Characterizations of Ultra-Large Reduced Graphene Oxide Monolayers. Chem Mater. 2009; 21: 5674-5680.

92. Khan U, O'Neill A, Lotya M, De S, Coleman JN. High-concentration solvent exfoliation of graphene. Small. 2010; 6: 864-871.

93. Alzari V, Nuvoli D, Scognamillo S, Piccinini M, Gioffredi E, Malucelli G, et al. Graphene-Containing Thermoresponsive Nanocomposite Hydrogels of Poly (N-isopropylacrylamide) Prepared by Frontal Polymerization. J Mater Chem. 2011; 21: 8727-8733.

94. Ghosh A, Subrahmanyam KS, Krishna KS, Datta S, Govindaraj A, Pati SK, et al. Uptake of H_2 and CO_2 by Graphene. J Phys Chem. 2008; 112: 15704-15707.

95. Ang PK, Chen W, Wee AT, Loh KP. Solution-gated epitaxial graphene as pH sensor. J Am Chem Soc. 2008; 130: 14392-14393.

96. Schedin F, Geim AK, Morozov SV, Hill EW, Blake P, Katsnelson MI, et al. Detection of individual gas molecules adsorbed on graphene. Nat Mater. 2007; 6: 652-655.

97. Dutta P, Horn PM. Low-frequency Fluctuations in Solids. Rev Mod Phys. 1981; 53: 497-516.

98. Sundaram RS, Gómez-Navarro C, Balasubramanian K, Burghard M, Kern K. Electrochemical Modification of Graphene. Adv Mater. 2008; 20: 3050-3053.

99. Liu Z, Robinson JT, Sun X, Dai H. PEGylated nanographene oxide for delivery of water-insoluble cancer drugs. J Am Chem Soc. 2008; 130: 10876-10877.

100. Sint K, Wang B, Král P. Selective ion passage through functionalized graphene nanopores. J Am Chem Soc. 2008; 130: 16448-16449.

101. Lanza M, Bayerl A, Gao T, Porti M, Nafria M, Jing GY, et al. Graphene-coated atomic force microscope tips for reliable nanoscale electrical characterization. Adv Mater. 2013; 25: 1440-1444.

102. Frammelsberger W, Benstetter G, Kiely J, Stamp R. C-AFM-Based Thickness Determination of Thin and Ultra-Thin SiO2 Films by Use of Different Conductive-Coated Probe Tips. App Phys Lett. 2007; 253: 3615-3626.

103. Castro Neto AH, Guinea F, Peres NMR, Novoselov KS, Geim AK. The Electronic Properties of Graphene. Rev Mod Phys. 2009; 81: 109.

104. Wen Y, Chen J, Guo Y, Wu B, Yu G, Liu Y. Multilayer graphene-coated atomic force microscopy tips for molecular junctions. Adv Mater. 2012; 24: 3482-3485.

105. Martin-Olmos C, Rasool HI, Weiller BH, Gimzewski JK. Graphene MEMS: AFM probe performance improvement. ACS Nano. 2013; 7: 4164-4170.

106. Shim W, Brown KA, Zhou X, Rasin B, Liao X, Mirkin CA, et al. Multifunctional cantilever-free scanning probe arrays coated with multilayer graphene. Proc Natl Acad Sci U S A. 2012; 109: 18312-18317.

107. Lanza M, Wang Y, Sun H, Tong YZ, Duan HL. Morphology and Performance of Graphene Layers on As-grown and Transferred Substrates. Acta Mech. 2014; 225: 1061-1073.

108. Lanza M, Porti M, Nafría M, Aymerich X, Whittaker E, Hamilton B. UHV CAFM Characterization of High-k Dielectrics: Effect of the Technique Resolution on the Pre- and Post-Breakdown Electrical Measurements. Microelectron Reliab. 2010; 50: 1312-1315.

109. Lanza M, Porti M, Nafría M, Aymerich X, Whittaker E, Hamilton B. Electrical Resolution during Conductive Atomic Force Microscopy Measurements under Different Environmental Conditions and Contact Forces. Rev Sci Instrum. 2010; 81: 106110.

110. Lanza M, Porti M, Nafría M, Aymerich X, Benstetter G, Lodermeier E, et al. Crystallization and Silicon Diffusion Nanoscale Effects on the Electrical Properties of Al2O3 Based Devices. Microelectron Eng. 2009; 86: 1921-1924.

111. Nafria M, Porti M, Bayerl A, Iglesias V, Lanza M, Martin-Martinez J, et al. Conductive Atomic Force Microscope as a Tool for the Characterization of Time-Dependent Variability of MOS Devices: Two Case Studies. International Semiconductor Device Research Symposium; Maryland, USA. 2013.

112. Fontsere A, Perez-Tomas A, Placidi M, Llobet J, Baron N, Lanza M, et al. Micro and Nano Analysis of 0.2 X mm Ti/Al/Ni/Au Ohmic Contact to AlGaN/GaN. Appl Phys Lett. 2011; 99: 213504.

113. Lanza M, Iglesias V, Porti M, Nafria M, Aymerich X. Polycrystallization effects on the nanoscale electrical properties of high-k dielectrics. Nanoscale Res Lett. 2011; 6: 108.

114. Lanza M, Iglesias V, Porti M, Nafria M, Aymerich X. Polycrystallization effects on the nanoscale electrical properties of high-k dielectrics. Nanoscale Res Lett. 2011; 6: 108.

115. Lanza M, Porti M, Nafría M, Aymerich X, Benstetter G, Lodermeier E, et al. Conductivity and Charge Trapping after Electrical Stress in Amorphous and Polycristalline Al2O3 Based Devices Studied with AFM Related Techniques. IEEE Transactions on Nanotechnology. 2011; 10: 344-351.

116. Lanza M, Wang Y, Bayerl A, Gao T, Porti M, Nafria M, et al. Tuning Graphene Morphology by Substrate towards Wrinkle-Free Devices: Experiment and Simulation. J Appl Phys. 2013; 113: 104301.

117. Aguilera L, Polspoel W, Volodin A, Haesendonck V, Porti M, Vandervorst W, et al. Nanoscale Effects of Annealing on the Electrical Characteristics of Hafnium Based Devices Measured in Vacuum Environment. Proc International Reliability Physics Symposium. 2008; 657-658.

118. Porti M, Nafria M, Aymerich X, Olbrich A, Ebersberger B. Electrical Characterization of Stressed and Broken Down SiO2 Films at a Nanometer Scale Using a Conductive Atomic Force Microscope. J Appl Phys. 2002; 91: 2071-2079.

119. Porti M, Avidano M, Nafria M, Aymerich X, Carreras J, Garrido B, et al. Nanoscale Electrical Characterization of Si-nc Based Memory Metal-oxide-semiconductor Devices. J Appl Phys. 2007; 101: 064509.

120. Lanza M, Gao T, Yin Z, Zhang Y, Liu Z, Tong Y, et al. Nanogap based graphene coated AFM tips with high spatial resolution, conductivity and durability. Nanoscale. 2013; 5: 10816-10823.

121. Chen YW, Prange JD, Dühnen S, Park Y, Gunji M, Chidsey CE, et al. Atomic layer-deposited tunnel oxide stabilizes silicon photoanodes for water oxidation. Nat Mater. 2011; 10: 539-544.

122. Kenney MJ, Gong M, Li Y, Wu JZ, Feng J, Lanza M. High-performance silicon photoanodes passivated with ultrathin nickel films for water oxidation. Science. 2013; 342: 836-840.

123. Chen T, Hu W, Song J, Guai G, Li C. Interface Functionalization of Photoelectrodes with Graphene for High Performance Dye-Sensitized Solar Cells. Adv Funct Mater. 2012; 22: 5245-5250.

124. Anish Madhavan A, Kalluri S, Chacko D, Arun T, Nagarajan S, Subramanian K, et al. Electrical and Optical Properties of Electrospun TiO2-Graphene Composite Nanofibers and Its Application as DSSC Photo-Anodes. RSC Adv. 2012; 2: 13032-13037.

125. Chen D, Zhang H, Liu Y, Li J. Graphene and Its Derivatives for the Development of Solar Cells, Photoelectrochemical, and Photocatalytic Applications. Energy Environ Sci. 2013; 6: 1362-1387.

126. Prasai D, Tuberquia JC, Harl RR, Jennings GK, Rogers BR, Bolotin KI, et al. Graphene: corrosion-inhibiting coating. ACS Nano. 2012; 6: 1102-1108.

127. Jardy A, Lasalle-Molin A, Keddam M, Takenouti H. Copper Dissolution in Acidic Sulphate Media Studied by QCM and RRDE Under AC Signal. Electrochim Acta. 1992; 37: 2195-2201.

128. Graf D, Molitor F, Ensslin K, Stampfer C, Jungen A, Hierold C, et al. Spatially resolved Raman spectroscopy of single- and few-layer graphene. Nano Lett. 2007; 7: 238-242.

129. Ferrari AC, Meyer JC, Scardaci V, Casiraghi C, Lazzeri M, Mauri F. Raman spectrum of graphene and graphene layers. Phys Rev Lett. 2006; 97: 187401.

130. Perkins W, Begeal D. Diffusion and Permeation of He, Ne, Ar, Kr, and D2 through Silicon Oxide Thin Films. J Chem Phys. 1971; 54: 1683-1694.

131. Hashimoto A, Suenaga K, Gloter A, Urita K, Iijima S. Direct evidence for atomic defects in graphene layers. Nature. 2004; 430: 870-873.

132. Rose F, Debray A, Martin P, Fujita H, Kawakatsu H. Suspended HOPG Nanosheets for HOPG Nanoresonator Engineering and New Carbon Nanostructure Synthesis. Nanotechnology. 2006; 17: 5192-5200.

133. Striemer CC, Gaborski TR, McGrath JL, Fauchet PM. Charge- and size-based separation of macromolecules using ultrathin silicon membranes. Nature. 2007; 445: 749-753.

134. Chen S, Brown L, Levendorf M, Cai W, Ju SY, Edgeworth J. Oxidation resistance of graphene-coated Cu and Cu/Ni alloy. ACS Nano. 2011; 5: 1321-1327.

135. Qi JS, Huang JY, Feng J, Shi da N, Li J. The possibility of chemically inert, graphene-based all-carbon electronic devices with 0.8 eV gap. ACS Nano. 2011; 5: 3475-3482.

136. Dubé C, Workie B, Kounaves S, Robbat A, Aksub M, Davies G. Electrodeposition of Metal Alloy and Mixed Oxide Films Using a Single-Precursor Tetranuclear Copper-Nickel Complex. J Electrochem Soc. 1995; 142: 3357-3365.

137. Poulston S, Parlett P, Stone P, Bowker M. Surface Oxidation and Reduction of CuO and Cu2O Studied Using XPS and XAES. Surf Interface Anal.1996; 24: 811-820.

138. Niaura G. Surface-enhanced Raman Spectroscopic Observation of Two Kinds of Adsorbed OH- Ions at Copper Electrode. Electrochim Acta. 2000; 45: 3507-3519.

139. Chou M, Liu S, Huang C, Wu S, Cheng C. Confocal Raman Spectroscopic Mapping Studies on a Single CuO Nanowire. Appl Surf Sci. 2008; 254: 7539-7543.

140. Sasi B, Gopchandran K. Nanostructured Mesoporous Nickel Oxide thin Films. Nanotechnology. 2007; 18: 115613.

141. Ishida Y, Mita Y, Kobayashi M, Endo S. Pressure Effects on Transition Metal Monoxide NiO. Phys Status Solidi B. 2003; 235: 501-504.

142. Mendoza L, Baddour-Hadjean R, Cassir M, Pereira-Ramos J. Raman Evidence of the Formation of LT-LiCoO2 Thin Layers on NiO in Molten Carbonate at 650^{O}C. Appl Surf Sci. 2004; 225: 356-361.

143. Kwon K, Kim SY. Extended Thermal Stability in Metal-Chloride Doped Graphene Using Graphene Overlayers. Chem Eng J. 2014; 244: 355-363.

144. Liang YQ, Yu LL, Cui ZD, Zhu SL, Li ZY, Yang, XJ, et al. Large-Scale Synthetic Graphene on Cu as Anti-Corrosion Coating by Chemical Vapor Deposition Approach. Science of Advanced Materials. 2014; 6: 545-549.

145. Nguyen BS, Lin JF, Perng DC. 1-nm-thick Graphene Tri-layer as the Ultimate Copper Diffusion Barrier. Appl Phys Lett. 2014; 104: 082105.

146. El-Adly RA, Youssef EA, El-Ghaffar MA. Use of a Multi-component Resin Produced from Petroleum Acid Sludge in Anti-corrosive Paints. Corros Prevent Contr. 1999; 46: 143-148.

147. Mittal V K, Bera S, Saravanan T, Sumathi S, Krishnan R. Rangarajan S,

et al. Formation and Characterization of Bilayer Oxide Coating on Carbon-Steel for Improving Corrosion Resistance. Thin Solid Films. 2009; 517: 1672-1676.

148. Redondo MI, Breslin CB. Polypyrrole Electrodeposited on Copper from an Aqueous Phosphate Solution: Corrosion Protection Properties. Corros Sci.2007; 49: 1765-1776.

149. Segarra M, Miralles L, Diaz J, Xuriguera H, Chimenos JM, Espiell F, et al. Copper and CuNi Alloys Substrates for HTS Coated Conductor Applications Protected from Oxidation. Mater Sci Forum. 2003; 426: 3511-3516.

150. Zhu S, Fillingim T, Robinson G. Flexible Simple Point-Charge Water in a Self-Supporting Thin Film. J Phys Chem. 1991; 95: 1002-1006.

151. Wang JY, Betelu S, Law BM. Line tension approaching a first-order wetting transition: experimental results from contact angle measurements. Phys Rev E Stat Nonlin Soft Matter Phys. 2001; 63: 031601.

152. Israelachvili JN. Intermolecular and Surface Forces. 2nd edn. Academic press. 1992.

153. Seemann R, Herminghaus S, Jacobs K. Dewetting patterns and molecular forces: a reconciliation. Phys Rev Lett. 2001; 86: 5534-5537.

154. Seemann R, Herminghaus S, Jacobs K. Gaining Control of Pattern Formation of Dewetting Liquid Films. J Phys Condens Matter. 2001; 13: 4925-4938.

155. Chen X, Wu J, Ma R, Hua M, Koratkar N, Yao S, et al. Nanograssed Micropyramidal Architectures for Continuous Dropwise Condensation. Adv Funct Mater. 2011; 21: 4617-4623.

156. Wei N, Lv C, Xu Z. Wetting of graphene oxide: a molecular dynamics study. Langmuir. 2014; 30: 3572-3578.

157. Ostrowski JH, Eaves JD. The tunable hydrophobic effect on electrically doped graphene. J Phys Chem B. 2014; 118: 530-536.

158. Chen Z, Dong L, Yang D, Lu H. Superhydrophobic graphene-based materials: surface construction and functional applications. Adv Mater. 2013; 25: 5352-5359.

159. Wei N, Peng X, Xu Z. Breakdown of fast water transport in graphene oxides. Phys Rev E Stat Nonlin Soft Matter Phys. 2014; 89: 012113.

160. Holt JK, Park HG, Wang Y, Stadermann M, Artyukhin AB, Grigoropoulos CP, et al. Fast mass transport through sub-2-nanometer carbon nanotubes. Science. 2006; 312: 1034-1037.

161. Cho J, Gao L, Tian J, Cao H, Wu W, Yu Q. Atomic-scale investigation of graphene grown on Cu foil and the effects of thermal annealing. ACS Nano. 2011; 5: 3607-3613.

162. Kirkland NT, Schiller T, Medhekar N, Birbilis N. Exploring Graphene as a Corrosion Protection Barrier. Corros Sci. 2012; 56: 1-4.

163. Podila R, Moore T, Alexis F, Rao AM. Graphene Coatings for Enhanced Hemo-compatibility of Nitinol Stents. R Soc Chem Adv. 2013; 3: 1660-1665.

164. Podila R, Moore T, Alexis F, Rao A. Graphene coatings for biomedical implants. J Vis Exp. 2013; : e50276.

165. Zhang W, Lee S, McNear KL, Chung TF, Lee S, Lee K, et al. Use of graphene as protection film in biological environments. Sci Rep. 2014; 4: 4097.

166. Li X, Cai W, Colombo L, Ruoff RS. Evolution of graphene growth on Ni and Cu by carbon isotope labeling. Nano Lett. 2009; 9: 4268-4272.

167. Cai W, Piner RD, Stadermann FJ, Park S, Shaibat MA, Ishii Y, et al. Synthesis and solid-state NMR structural characterization of 13C-labeled graphite oxide. Science. 2008; 321: 1815-1817.

168. Obraztsov A, Obraztsova E, Tyurnina A, Zolotukhin A. Chemical Vapor Deposition of Thin Graphite Films of Nanometer Thickness. Carbon. 2007; 45: 2017-2021.

169. Reina A, Son H, Jiao L, Fan B, Dresselhaus MS, Liu Z, et al. Transferring and Identification of Single- and Few-Layer Graphene on Arbitrary Substrates. J Phys Chem C. 2008; 112: 17741-17744.

170. Schriver M, Regan W, Gannett WJ, Zaniewski AM, Crommie MF, Zettl A, et al. Graphene as a long-term metal oxidation barrier: worse than nothing. ACS Nano. 2013; 7: 5763-5768.

171. Topsakal M, Sahin H, Ciraci S. Graphene Coatings: An Efficient Protection from Oxidation. Phys Rev B. 2012; 85: 155445.

172. Singh Raman RK, Chakraborty Banerjee P, Lobo DE, Gullapalli H, Sumandasa M, Kumar A, et al. Protecting Copper from Electrochemical Degradation by Graphene Coating. Carbon. 2012; 50: 4040-4045.

173. Zahran RR, Ibrahim IH, Sedahmed GH. The Corrosion of Graphite/Copper Composites in Different Aqueous Environments. Mater Lett. 1996; 28: 237-244.

174. Lanza M, Wang Y, Gao T, Bayerl A, Porti M, Nafria M, et al. Electrical and Mechanical Performance of Graphene Sheets Exposed to Oxidative Environments. Nano Res. 2013; 6: 485-495.

175. Wei Y, Wu J, Yin H, Shi X, Yang R, Dresselhaus M. The nature of strength enhancement and weakening by pentagon-heptagon defects in graphene. Nat Mater. 2012; 11: 759-763.

176. Huang PY, Ruiz-Vargas CS, van der Zande AM, Whitney WS, Levendorf MP, Kevek JW, et al. Grains and grain boundaries in single-layer graphene atomic patchwork quilts. Nature. 2011; 469: 389-392.

177. Yu Q, Jauregui LA, Wu W, Colby R, Tian J, Su Z, et al. Control and characterization of individual grains and grain boundaries in graphene grown by chemical vapour deposition. Nat Mater. 2011; 10: 443-449.

178. Yazyev OV, Louie SG. Electronic transport in polycrystalline graphene. Nat Mater. 2010; 9: 806-809.

179. Grantab R, Shenoy VB, Ruoff RS. Anomalous strength characteristics of tilt grain boundaries in graphene. Science. 2010; 330: 946-948.

180. Kim P. Graphene: Across the border. Nat Mater. 2010; 9: 792-793.

181. Hui F, Shi Y, Ji Y, Lanza M, Duan H. Mechanical Properties of Locally Oxidized Graphene Electrodes. Arch Appl Mech. Accepted for publication.

182. Wu ZS, Ren W, Gao L, Zhao J, Chen Z, Liu B, et al. Synthesis of graphene sheets with high electrical conductivity and good thermal stability by hydrogen arc discharge exfoliation. ACS Nano. 2009; 3: 411-417.

183. Liu Q, Ren W, Li F, Cong H, Cheng HM. Synthesis and High Thermal Stability of Double-Walled Carbon Nanotubes Using Nickel Formate Dihydrate as Catalyst Precursor. J Phys Chem C. 2007; 111: 5006-5013.

184. Huang H, Kajiura H, Tsutsui S, Murakami Y, Ata M. High-Quality Double-Walled Carbon Nanotube Super Bundles Grown in a Hydrogen-Free Atmosphere. J Phys Chem B. 2003; 107: 8794-8798.

185. Strong V, Dubin S, El-Kady MF, Lech A, Wang Y, Weiller BH, et al. Patterning and electronic tuning of laser scribed graphene for flexible all-carbon devices. ACS Nano. 2012; 6: 1395-1403.

186. Lee JH, Lee EK, Joo WJ, Jang Y, Kim BS, Lim JY, et al. Wafer-scale growth of single-crystal monolayer graphene on reusable hydrogen-terminated germanium. Science. 2014; 344: 286-289.

187. Ball SC, Hudson SL, Thompsett D, Theobald B. An Investigation into Factors Affecting the Stability of Carbons and Carbon Supported Platinum and Platinum/cobalt Alloy Catalysts During 1.2 V Potentiostatic Hold Regimes at a Range of Temperatures. J Power Sources. 2007, 171: 18-25.

188. Li H, Cheng N, Zheng Y, Zhang X, Lv H, He D, et al. Oxidation Stability of Nanographite Materials. Adv Energy Mater. 2013; 3: 1176-1179.

189. Lee MS, Lee K, Kim SY, Lee H, Park J, Choi KH, et al. High-performance, transparent, and stretchable electrodes using graphene-metal nanowire hybrid structures. Nano Lett. 2013; 13: 2814-2821.

Ann J Materials Sci Eng - Volume 1 Issue 3 - 2014
ISSN : 2471-0245 | www.austinpublishinggroup.com

Citation: Hu J, Ji Y, Shi Y, Hui F, Duan H and Lanza M. A Review on the use of Graphene as a Protective Coating against Corrosion. Ann J Materials Sci Eng. 2014;1(3): 16.